Natural Resources Canada | Ressources naturelles Canada

GEOLOGICAL SURVEY OF CANADA
OPEN FILE 7618

Refraction seismic velocity analyses from multichannel seismic data acquired during Expedition ARA04C on the IBRV Araon in the Beaufort Sea

M. Riedel., J. K. Hong, Y. K. Jin, H. S. Kim

2014

Canada

GEOLOGICAL SURVEY OF CANADA
OPEN FILE 7618

Refraction seismic velocity analyses from multichannel seismic data acquired during Expedition ARA04C on the IBRV Araon in the Beaufort Sea

M. Riedel[1], J.K. Hong[2], Y. K. Jin[2], H. S. Kim[3]

[1] Natural Resources Canada, Geological Survey of Canada, 9860 West Saanich Road, Sidney, British Columbia
[2] Korea Polar Research Institute (KOPRI), 26 Songdomirae-ro, Yeonsu-gu Incheon, 406-840, Korea
[3] Korea Gas Corporation, 5th Floor, Korea Paperless Trade Centre, 688 Sampyeong-dong, Bundang-gu, Seongnam-si, Gyeinggi, Korea

2014

doi:10.4095/295549

This publication is available for free download through GEOSCAN (http://geoscan.nrcan.gc.ca/).

Recommended citation
Riedel, M., Hong, J. K., Jin, Y. K., and Kim, H. S., 2014. Refraction seismic velocity analyses from multichannel seismic data acquired during Expedition ARA04C on the IBRV Araon in the Beaufort Sea; Geological Survey of Canada, Open File 7618, 67p. doi:10.4095/295549

Publications in this series have not been edited; they are released as submitted by the author.

Abstract

Expedition ARA04C (conducted from September 10 – September 26, 2013 in Canadian waters) on the Korean icebreaker IBRV Araon was laid out to investigate the Beaufort Sea shelf and slope region and collect geo-scientific data for various aspects relevant to the GSC's mandated regional geo-hazard assessment of the offshore Beaufort region. A critical element of the geo-hazards is the distribution of permafrost across the submerged shelf. To address this question and to verify data from earlier attempts made by the GSC in the mid 1980ies, a set of multichannel seismic (MCS) lines were collected across and along the shelf edge. Refracted arrivals were picked on all MCS lines acquired and velocities for the first and where occurring, second and even third refractions were determined. The depth to the first refractor was determined using simple ray-path geometry for a refracted, planar 2 layer case, with a fixed velocity of the upper layer (ocean water) of 1450 m/s determined from measurements of physical properties in the water column using a standard Conductivity-Temperature-Depth (CTD) tool. Using this velocity value creates a fully flat direct arrival when the shot-gather is reduced by this velocity value, confirming that this value is appropriate. Depths to 2nd or 3rd refractor where not determined in this study. Arrivals from deeper refractions are often masked by the occurrence of refractions generated by multiples and from strong linear noise occurring along the streamer. The results from the refraction velocity analysis allow verification of major boundaries of permafrost or ice-bearing sediment occurrences from previous work, but also define several critical corrections, especially near the shelf edge zone. Correlation of the MCS refraction data and the coincident 3.5 kHz sub-bottom profiler data reveal that a regional unconformity (~5 to ~15 meter below seafloor) often is the source of the first detectable refraction instead of the seafloor.

1 Introduction

A two-ship scientific research expedition in the southern Beaufort Sea was carried out between September 10 to October 10, 2013, using the research icebreaker Araon operated by the Korea Polar Research Institute (KOPRI) and the Canadian Coast Guard Ship (CCGS) Sir Wilfrid Laurier. The multidisciplinary science program included geological, geophysical, and oceanographic investigations of the continental shelf and slope. The research conducted will help improve the understanding of geohazards in this setting by assessing the regional geology, the stability of decomposing offshore permafrost and gas hydrates, mechanisms for surficial gas/fluid migration, and active geologic processes. Priorities for the Araon Expedition ARA04C (see Figure 1 for a complete ship track) included a multi-channel seismic (MCS) survey and detailed bathymetric mapping with high-resolution sub-bottom profiling with the goal to collect site-survey data supporting the Integrated Ocean Drilling Program (IODP) pre-proposals 806 (Dallimore et al., 2012) and 753 (O'Regan, et al. 2010). The site-survey data are required to define drill site locations for safe operations and to ensure, science goals are met. Therefore, the seismic lines must be acquired in a systematic grid-pattern of perpendicular lines crossing the shelf edge and lines parallel to the shelf edge. Prior to the Expedition ARA04C, the science teams met to discuss the requirements for the seismic survey and worked with industry partners, supporting the effort through their 3D seismic data sets in deep-water to optimize the layout. Industry well locations with high quality well logs allowing the definition of the base of permafrost as well as stratigraphic information were used as tie-points of the main IODP transects for pre-proposal 806. In total, five transects were defined (color-coded for simplicity) and are shown in Figure 2 with respect to the main bathymetric features and permafrost distribution in the study area. In order of priority, the transects are "red", "yellow" "blue", "cyan", and "white". Around each of these transects a set of parallel and perpendicular lines would suffice for the IODP site survey data. The MCS data acquisition is complemented by the deployment of eight Ocean Bottom Seismometers (OBS) to further allow detailed velocity determination. However, results from the OBS analyses are not included in this study.

Ice conditions were unexpectedly severe in 2013 and ice distribution was much further to the south and often covered the shelf edge zone. Seismic data acquisition was changed routinely to avoid damage of the seismic systems by ice-collisions and to simultaneously maintain as much as possible of the scientific goals related to IODP site survey grid lines, but most of the eastern

portion of the study was inaccessible during the month of September 2013. Figure 3 shows the distribution of all lines acquired during Expedition ARA04C. Much of the data acquisition was limited to a narrow zone between the “red” and “yellow” transects in the east and west, respectively, as well as the ice-limit to the north and permit-limitations (50 m isobaths) to the south. At the beginning of Expedition ARA04C most of the Mackenzie trough region was ice-free that would have allowed seismic data acquisition in support of IODP pre-proposal 753, but the decision was made to start as far east as possible and acquire data for IODP pre-proposal 806 first, and work the survey back west as time progresses. However, by the end of the expedition, the northern portion of the Mackenzie trough region across most of the Chevron 3D block area was ice-covered (50-80%), which precluded seismic data acquisition over the proposed drill locations. However, multi-beam bathymetry mapping, sub-bottom profiling, as well as gravity coring and oceanographic data collection were performed in support of IODP pre-proposal 753 (see Figure 1 for overview of stations visited).

In this study, we show the results of using the MCS data from Expedition ARA04C to define the seismic velocity structure from refracted arrivals. The velocities are then used to delineate the sub-seafloor permafrost distribution along all lines acquired during Expedition ARA04C. Results from this work are compared to a previous such study by Pullan et al. (1987) who also measured seismic velocity from refracted arrivals on a grid of industry MCS data on the shelf. The work by Pullan et al. (1987) was unfortunately never published in the peer-reviewed scientific literature, but is available as part of the Geological Survey of Canada Marine Science Atlas of the Beaufort Sea. One goal of our new study is to verify the location of major boundaries defined in the map of permafrost distribution, and to better understand the thresholds used to define these boundaries.

2 Data acquisition and technology

2.1 Airgun array and streamer

The MCS systems on the IBRV Araon consist of an eight-gun airgun array, a streamer, two compressors, as well as survey control and data acquisition units (Figure 4). The airgun array consists of eight Sercel G-Guns and a float that maintains the source depth at 6 meters below sea-surface. The airguns have four different volumes: gun 1 and 2 were 250 in^3, gun 3 and 4 were 200 in^3, gun 5 and 6 were 90 in^3 and gun 7 and 8 were 60 in^3. The total volume of the source is thus 1200 in^3 (equivalent to 19.7 liter). The streamer consists of ten solid sections with a total of 120 channels. The hydrophone group interval is 12.5 meter. The total length of the streamer is 1.8 km including the tail buoy, fluid stretch-section and a lead-in cable section. Eight cable levelers (birds) are attached on the streamer every 300 meters that maintain the streamer depth in the water. Figure 5 shows a diagram of the important geometry definitions required for data processing. The compressor system of the IBRV Araon consists of two compressors, which are alternated every 12 hours. The working pressure is set between 120 to 150 bar (1,740 – 2030 psi).

The survey control system onboard the vessel consists of a navigation control system, an airgun controller, a bird controller, a recording system, a quality control system and a navigation editing system. The navigation system (NaviPac) defines the seismic line geometry and controls the shooting interval according to a set shot interval distance, and is linked to the gun controller and recording system. The airgun controller (Bigshot) receives the event signal from the NaviPac and triggers the airgun array. The Bigshot system displays the shooting timing, quality, and wave shape for each used airgun. The bird controller defines streamer depth and displays the location and heading of birds. The recording system (Baby Seal from Sercel), records seismic data and sends them to the final storage system. A quality control system (e-SQC pro from Sercel) displays the real time data for each shot gather and also displays a running window of the near trace gather (trace 1). The navigation editing system (NaviEdit from EIVA) transforms the NaviPac survey file to a standard navigation file (UKOOA P1/90) for final use.

The multi-channel seismic survey was conducted September 14 to September 21, 2013. The seismic data set collected consists of a total of 14 survey lines, with 435 line-km, and 4,564 individual shot-gathers. The shooting interval was set to 93.75 meter at a ship speed of ~4.5 knots and the fold (number of traces within a common-mid-point) of the survey at optimal

conditions was eight. The complete acquisition parameters are summarized in Table 1. During the survey, the compressors were several times unable to maintain the desired working pressure above 140 bar due to air leakage at the airgun array. The airgun array was thus constantly modified by reducing total volume and number of airguns fired to air-volumes that allow the compressors to better maintain the desired working pressure. However, air-leakage was pervasive throughout the survey, which was interrupted several times to allow for airgun-array repairs.

2.2 Ice conditions

Additional complexities for the seismic survey arose from the wide-spread ice-cover of the desired survey area. Ice-monitoring with the bridge's radar system was effective in avoiding major ice problems throughout the seismic survey. Line-orientation and distribution were planned no longer than 24 hours in advance using the Canadian Ice-service maps as general guidelines. However, the maps proved too coarse for detailed planning. Wind and surface current speeds were modifying the actual ice distribution faster than anticipated. The survey thus fell ultimately short in covering the originally desired area, especially over the eastern portion of the study area.

2.3 Marine Mammal Observations

The seismic survey was also conducted following the mandated marine mammal observation guidelines and mitigation measures as per environmental permit granted by the Environmental Impact Screening Committee (EISC). Three marine mammal observers continuously monitored the area around the vessel during day-light hours. Prior to any start of the airgun array, a one-hour pre-shooting watch established that no marine mammals were within the permitted exclusion zone (1500 m radius around the vessel). The airgun array was then fired one gun at a time over a total of 45 minutes to one hour until the maximum sustainable air-volume was reached. Seismic data acquisition could then commence also during night-time or times of low visibility, if no marine mammal sightings were made in the hour prior to limitations of visibility (i.e. darkness or fog). Several bowhead whale aggregations zones were defined by the Department of Fisheries and Oceans and seismic operations could only be made during day-light within these zones, provided no mammal is within the exclusion zone itself. Throughout the entire seismic survey in September 2013, no interruptions from marine mammals occurred as no mammals were seen at all in the vicinity of the vessel while the airgun array was used.

3 Seismic data processing, geometry definition, and seismic refraction method

3.1 Processing sequence

The MCS data are initially stored in SEGD format as individual shot-gathers. Each shot gather contains 120 channels of actual seismic data as well as one auxiliary trace. A simple processing sequence was designed using the seismic processing package Globe-Claritas available at the Pacific Geoscience Centre, consisting of:

- SEGD-data reading;
- Checking header to identify live traces and removal of auxiliary traces;
- General de-bias of data traces (removing any DC component over the entire recording time window of 10 seconds);
- Bandpass filtering over a broad frequency range (6 – 12 – 380 – 460 Hz) to only remove low-frequency flow-noise on streamer;
- Adding geometry (offset, source, receiver and common-mid-point locations)
- Writing of output file using standard SEGY-data format and truncation of trace length to 3 seconds (reducing data volume), optimized for (a) shallow reflection seismic processing and (b) refraction seismic analysis;
- For the picking and velocity best-fit ruler-technique, an automatic gain control (100 ms window length) was applied within the picking window to optimize visibility of the first arrival.;
- The data was further reduced by the water velocity (1445, or 1450 m/s) for simpler identification of the refraction.

3.2 Geometry

The survey line geometry was defined for each line individually. The original line-geometry was provided by the navigation editing system in UKOAA standard with shot latitude and longitude values reported in degrees-minutes-seconds. Geometry definition within Globe-Claritas is based on a coordinate system in meters, and requires a conversion of the UKOAA files into individual survey (sur) and observer (obl) files. A series of simple Fortran-77 codes were first written for this purpose to (a) extract the coordinate information from the UKOAA files, (b) transform those into UTM coordinates, and (c) write the formatted survey and observer files. After editing of these files to match expected formatting standards using acsii-to-sur and

ascii-to-obl file format routines in Globe-Claritas, a crooked-line geometry was defined for each line as line-orientation was not always entirely straight (due to varying weather- (wind and wave direction) and ice-conditions). As the geometry information is input into trace header words of limited storage capacity for the six or seven digits long coordinate values of easting and northing, the coordinates were reduced by subtracting a common large value (e.g. 480,000 for all easting values).

3.3 Refraction Method

Seismic refraction is a technique commonly used in exploration or geophysical engineering applications. A seismic wave emitted from a source travels through the subsurface and when this wave front hits an interface at the critical angle (defined by Snell's law) it travels along this interface at a velocity of the underlying medium (V_2). It is necessary that the velocity of the layer below the interface is higher than the velocity above (V_1), (Figure 6). Plotting the arrival times of the wave fronts as function of offset as they are received at geophones or (as in our case) hydrophones in the streamer, shows that refracted arrivals arrive earlier than the direct arrival beyond a critical distance, which is called the cross-over-point (Figure 7). The arrival times of the direct and refracted waves are aligning linearly in the offset-time diagram (or shot-gather) and the slope of the arrival times is equivalent to the slowness (inverse of velocity).

After the seismic data were written to disk (SEGY standard) including the offset information for each trace, the First-Break Static tool in Globe-Claritas was used to visualize the shot gathers and pick the refracted arrivals. Defining the refracted wave velocity was done by using a ruler tool to define a best-fit line to the first arrivals of the refracted wave and measuring the cross-over distance (point upon which the refracted wave arrives earlier than the direct wave through the water). This was done for all shot gathers along the 14 lines acquired.

In order to make the picking process easier for the interpreter, the shot gathers were reduced by the water-velocity. The water velocity is defined to be on average 1450 m/s from water-column measurements using standard Conductivity-Temperature-Depth (CTD) profiling. This reduction results in the direct arrival to be horizontal in the shot gather.

4 Results

4.1 Previous work and location of new data relative to existing boundaries

The study by Pullan et al. (1987) defines boundaries between three major domains of offshore permafrost occurrence, using a threshold in seismic velocity of 2500 m/s (Figure 9a). In their analyses, the velocity of ice-bearing sediments ranges from ~1800 m/s to ~4500 m/s. A zone of continuous permafrost with velocities consistently over 2500 m/s occurs in the southern portion of the shelf region (blue-colored zone in Figure 9a), surrounded by a zone of discontinuous permafrost distribution (pink-colored zone in Figure 9a), and a fringe of sediments with low ice content (yellow-colored zone in Figure 9a). The locations of the 14 lines acquired during Expedition ARA04C cross the boundary between the zone of discontinuous permafrost and the zone of sediments with low ice content. The zone of continuous permafrost occurs in water depths of less than 50 m over the accessible study region in September 2013 and thus this region could not be further investigated.

Line-1 and Line-22 cross the shelf edge at the eastern portion of the study zone where pingo-like features (PLF) are widespread (Figure 9b). Data from these two lines provide important information on the velocity distribution of ice-bearing sediments of those portions of the shelf edge that have yet not experienced any recent slope failure. Only one line (Line-12) crosses the shelf edge over the major slump-feature seen on the multi-beam data (Figure 9b) on the western edge of the study zone. Due to sudden ice occurrence, Line-3 was shortened and did not cross the shelf edge completely so that Line-4 is located about parallel to the zone of PLFs. After completing Line-5 the airgun leakage became too severe and despite two attempts in reducing air-volumes during Line-6 and Line-7, the survey was interrupted for a day to repair the airgun array. The survey was restarted to acquire lines parallel to the shelf edge (Line-8 and Line-10). Line-11 and Line-12 are in a zone where Pullan et al. (1987) defined no or little ice content in the sediments. During the end of Line-12 the airgun leakage was again too severe and the survey was interrupted for 1.5 days. Due to a change in ice cover it was possible to extend the survey area further to the east and one main line along the highest priority “red” transect was attempted. Line 21 started the line from the south-east, but airgun problems and increasing wave height and wind speed resulted in a halt of the survey over night with the streamer deployed but the airgun array on deck. The survey was re-started at Line-22, but ultimately abandoned half

way across the intended line-length due to repeated airgun failure and almost complete loss of pressure in the system.

4.2 Results from individual lines of Expedition ARA04C

The individual velocity values obtained for each line are shown in Figure 10 as function of shot number along each profile. Depth of the first refractor is also shown along each profile, together with the seafloor depth as determined from the MCS data (trace 1) and adjusted for the towed streamer and array (at 6 meter below sea-surface). For the definition of the seafloor (and comparison to depth to first refractor), the seafloor reflection of the first trace was picked and converted to depth after a trigger-time delay of 60 ms was removed from the traces. The delay was possible to define for all shots that overlap with an existing 3D seismic data set and through comparing the depths to the coincident 3.5 kHz sub-bottom profiler data.

The velocity values and cross-over distances picked by hand with the ruler-tool in the Refraction Statics tool of Globe Claritas are rounded to an accuracy of 5 m/s and 5m, respectively (e.g. a velocity from the best linear fit of 2343.2 m/s is reported as 2345 m/s). Line 7 is very short and has multiple airgun shot failures (and the survey was interrupted for repairs after this line) and due to the location parallel and close to Line 10, the few velocity results are not presented here. A map-view of these sparse lines to produce contour-lines of velocity thresholds is not possible at this point. We therefore only display the velocity profiles superimposed on the main map by Pullan et al., (1987).

4.2.1 Line-1

Velocity from the first refractor and second refractor along this line are almost always higher than the 1800 m/s threshold used by Pullan et al. (1987) as indicator for some ice within sediments (Figure 10a). Velocities on this line are above the threshold of 2500 m/s (blue solid line) used to define zones of continuous permafrost by Pullan et al. (1987) for about 2/3 of the shots analysed. A zone of velocity values below the 2500 m/s threshold in the SE corner of the line (where one would initially expect higher velocity values) coincides with the sediment-filled Kugmallit-Trough, which has been formed only since the last glaciation. The trough has therefore experienced erosion and re-deposition of recent marine sediments all without ice-contact and the “warming” of the seafloor and thawing of permafrost has therefore been more advanced than in other regions unaffected by Holocene shelf processes. The depth to the top

refractor in the zone of the Kugmallit-Trough is overall deeper than along the remaining line (Figure 10b). At the NW portion of the line in deeper water exceeding 80 m and across the area with abundant PLFs, the first refractor almost always is the seafloor itself with velocities around 2000 m/s. This may indicate some ice is present at and near the seafloor (the water temperature in this zone is below 0 degrees Celsius) or may correlate to the underlying unconformity (consisting of harder, more consolidated sediments). Overall, the new velocity values confirm the previously mapped boundary between discontinuous ice-bonded sediments and sediments with low ice-content to within ~1km (Figure 11a).

4.2.2 Line-2

This short E-W segment shows velocity above the threshold of 1800 m/s (Figure 10c) with the exception of a short 800m long interval between shots 2208 and 2216, where velocities of the first refractor are as low as 1700 m/s. Along this line, depth to the refractor is on average 10 – 20 mbsf (Figure 10d), with the exception of several valleys, correlating to sediment-filled channels (like the Kugmallit-Trough). The 3.5 kHz sub-bottom profiler data show the prominent erosional unconformity below the seafloor at ~10-15 mbsf, which seems to correlate well to the occurrence of the refraction. The refraction from the seafloor is therefore not measured as it may be immediately over-whelmed by the faster arrivals from underneath. With trace-spacing of 12.5 m along the streamer it may be impossible to identify the first refraction, if e.g. it occurs only on one or two traces prior to the arrival of the faster wave-front from the underlying unconformity. This already points to a complexity in the interpretation of these data as sediments with some ice content cannot easily be separated on seismic velocity alone from older, more consolidated sediments underneath the unconformity, which could be ice-free. Access to core with intact ice-content would be required to address this issue.

4.2.3 Line-3

Line-3 is a transect parallel to Line-1 and shows a marked decrease in seismic velocity from SE to NW (Figure 10e). Velocity values drop below the 2500 m/s around shot point 3200 and, with the exception of two short segments, remain below this threshold for the remainder of the line. The interval between shot 3320 and 3330 corresponds to a zone already indicated on the map by Pullan et al. (1987) as possibly being patchy permafrost (pink-colored zone) as seen in Figure 11b. However, the segment between shots 3283 and 3269 with even higher velocity values did not exist on the previous map by Pullan et al. (1987), which upon closer inspection of

the original line-distribution in the map presented in the Marine Science Atlas of the Beaufort Sea is caused by no coverage. Towards the NW end of the line, a PLF feature was imaged and velocities surrounding the PLF increase from a background of ~1800 m/s towards both sides to over 2200 m/s in the centre of the PLF feature. As these PLF features are known to contain ice-bearing sediments, this increase in velocity is probably also ice-related and not related to the unconformity as mentioned earlier.

4.2.4 Line-4

Line-4 was shot along the shelf edge across the PLF landscape. The previous Line-3 was abruptly terminated due to the occurrence of sea-ice, and Line-4 was inserted into the survey grid to maintain a regular acquisition pattern across the deployed ocean bottom seismometers. Thus, portions of the start and end of the line are affected by rapid turning of the vessel and crooked streamer geometry. Data from these portions should not be interpreted. 17 shots could not be fired and for ~60 shots, no refraction was seen at all. Thus the data set is rather limited and if a refracted arrival was detected, the velocity is mostly below the 1800 m/s threshold (Figure 10g). Although velocity values appear relatively consistent with few variations, the depth of the refractor is scattered. This is likely the result of quite uncertain cross-over distance. The complicated seafloor topography with many PLF features and gullies probably creates complex overlapping wave fronts not really suitable for refraction work.

4.2.5 Line-5

Line-5 crosses from the NW from an area previously determined as ice-free to a zone with low ice-content, to the discontinuous ice-bonded sediments. Velocities along this line (Figure 10i) are over the threshold of 1800 m/s between shots 5045 and 5080 and then again 5225 and 5295 before a large step occurs and velocity values are sharply increasing to over 3000 m/s near shot point 5360. The second step over the 1800 m/s threshold (shot 5225 to 5295) is at the boundary previously identified by Pullan et al. (1987), as well as the sharp increase at shot point 5360 (Figure 11c). The depth of the refractor is relatively consistent along this line (Figure 11j) and is on average between 15 and 20 mbsf. Several undulations to larger depths in this surface results from small sediment-filled channels.

4.2.6 Line-6

Along this short line, which was overall very noisy and further reduced in quality due to the varying streamer depth at the turns at the start and end of the profile, the velocity shows large

variations. Zones of velocity values below the 1800 m/s threshold are from the seafloor but some portions of the line show refractions with velocities above the 2500 m/s threshold (Figure 10k). Refractor depths vary accordingly along this line (Figure 10l). Due to the shortness of the line and airgun volume problems, no further analyses and comparisons to the 3.5 kHz data were undertaken. Also, the following Line-7 is skipped (only 17 useful shots out of 40 total shots) in this study. Regionally, Line 7 is close (and parallel) to Line 10 (see below).

4.2.7 Line-8

Line-8 was started in the west after a major airgun-overhaul to acquire a line parallel to the slope and to cross major boundaries between supposedly ice-free to discontinuous ice-bonded sediments (Figure 9a). Velocity values vary significantly along the line (Figure 10m). The depth of the first refractor (Figure 10n) varies between depths at the seafloor and a depth-range bracketing the regional unconformity (about 15-20 mbsf). Several deeper valley-like depressions also are also occurring that were linked to channels with recent sediment fill in the 3.5 kHz data. Boundaries between zones of varying ice-content previously mapped by Pullan et al. (1987) are generally confirmed by the new velocity analysis (Figure 11d).

4.2.8 Line-9

The N-S trending Line-9 is within the zone of discontinuous ice-bonded sediments (Figure 9a). The velocity of the first refractor (Figure 10o) varies rapidly and crosses the 1800 m/s and 2500 m/s threshold at several locations. Depth to the first refractor (Figure 10p) is varying in depth accordingly, mimicking to some degree the topography superimposed on the seafloor (and underlying unconformity) by small-scale sediment-filled channels.

4.2.9 Line-10

Line-10 (going E-W) starts in the area of discontinuous permafrost (pink zone in Figure 9a) and the velocity obtained (Figure 10q) along this line stays (with the exception of a short segment between shots 10080 and 10100) above the 2500 m/s threshold. Velocity values are scattered though with values as high as 4400 m/s. Depth to the refractor (Figure 10r) is generally close to (or at) the seafloor, with several depressions that were linked to sediment-filled channels (compare to Figure 12a). The boundaries between the zone of discontinuous ice-bonded sediments and sediments with low- to no-ice content (threshold at 2500 m/s and 1800 m/s, respectively) at the western end of the line were confirmed with the new velocity analysis (Figure 11e) although two shorter segments with velocity values below or around the 1800 m/s

threshold exist in what was mapped as homogenous zone of “discontinuous” ice-bonded sediments. These “holes” in the ice-content linked to channels with recent sediment fill are in general not contradicting the definition of discontinuous ice-bonded sediments and no changes to the map are warranted.

4.2.10 Line-11

This line going from the SE to the NW shows velocity values for the first and second refractor continuously below or close to the 1800 m/s threshold (Figure 10s) confirming its location in a zone as defined as mostly low- to no-content sediments. However, towards the end of the line, a zone of much elevated velocities exists exceeding the 2500 m/s threshold (shots 11230 to 11245). Here, a clear match in refractor depth to either being at the seafloor or the unconformity was found (Figure 12c). The high velocity patch correlates to a loss in acoustic penetration of the 3.5 kHz sub-bottom profiler record, indicating that there is some increase in ice-content in that zone. It is also important to note that the velocity of the first refraction detected (independent of it being the seafloor or unconformity) away from the patch of high velocity does not vary significantly and is always below 1800 m/s. Also, the second refraction found in this area is well below the same threshold. Thus, the unconformity itself can be ruled out as a source for a high velocity contrast.

4.2.11 Line-12

Line-12 shows low velocities below both thresholds (Figure 10u), confirming the previous map by Pullan et al. (1987). Towards the NW portion of the line, the acquisition geometry with the airgun located over deeper water than the streamer effectively represents an up-dip shooting experiment and thus the measured velocities are too high. The depth to the refractor is therefore calculated at values shallower than the seafloor itself (Figure 10v). A bright-spot (though no polarity reversal occurs) is identified close to the shelf edge, coinciding with a bright reflection in the 3.5 kHz data and loss of acoustic penetration (Figure 12d). However, no increase in refraction velocity was detected, but a deepening of the surface to the top of the refraction.

4.2.12 Line-21

Line-21 has only a limited number of successful shots and the data from this line are sparse. However, the few shots that were fired generated a surprising consistent result, in that the velocities are above the 2500 m/s threshold, and often higher than 3000 m/s (Figure 10 w). The

depth to the refractor is calculated on average at 170 m below source, which is about 90 m below seafloor (Figure 10x). This consistently high velocity suggests a change to the map by Pullan et al (1987), but without a careful analysis of the older lines and checking why the area was identified as discontinuous permafrost (pink colored zone in Figure 9a) and not as continuous permafrost (blue colored zone in Figure 9a). Also, log-data from well Nerlerk M-98 could be used to verify the permafrost occurrence.

4.2.13 Line-22

Line-22 started in the NW in deep water and was intended to image the shelf break zone and identify the onset of permafrost near the PLF occurrences. The first refractions were recorded on the streamer at shot 22225, about 19km into the line. The airgun array was performing quite well but already after 120 shots the first difficulties with keeping the working pressure were reported and gun volumes were modified. Throughout the remainder of the line, effective array-volume size was modified continuously, creating rather difficult conditions for consistent seismic imaging and detection of refractions, especially when the airgun volumes were small. Nonetheless, the velocity data from this line (though patchy and probably associated with a larger error than on other lines) show a progressive increase in velocity from the deeper offshore portion (north of the PLF zone) to the shallower shelf portion in the south (Figure 10y). Accordingly, along the first third of the line, the first refractor detected is effectively the seafloor itself (Figure 10z), although the down-shoot geometry of the acquisition resulted in false velocity values on the slope region (the streamer is over deeper water than the airgun source) and the depth of the refractor is placed below the seafloor. Also, the considerable slope angle shifts the image-points on the seafloor down-slope, so that the impression is created that the refractions is from greater depth. No geometric corrections have been applied at this stage and likely are not required for future work as this region is outside the zone of permafrost interest. Results from this Line-22 match the pre-existing map and inferred distribution of ice-bearing sediments (Figure 9a).

5 Discussion and error definition

The refraction technique using simple linear best-fit approximation to the arrival times is technically only valid for simple planar geometry of a layered sub-seafloor system, and thus over-simplistic for some regions shown in this study. Any dip on the seafloor or sub-seafloor layers creates apparently higher or slower velocity values that are not representing the true in situ velocity (and thus inferred ice-content or permafrost distribution). In the case of this study, almost all lines are situated on the shelf with an overall seafloor dip of less than one degree. However, sub-seafloor channels, PLFs, and taliks create rapidly changing, rough surfaces below the seafloor and thus could generate false velocity values. This may also be the reason for the relative high scatter (variation from shot to shot) seen in the inferred refraction velocity values obtained along all lines. Additionally, the technique used in this study is not fully appropriate for gradient zones and although (where possible) a piece-wise linear approximation was used to represent a layered sub-surface structure when a gradually changing refraction was identified it is only an approximation to the true geology.

Errors to the velocity calculation can have several origins:

(a) Interpreter error in picking velocity through the linear-fit ruler-technique

(b) Interpreter error in defining the cross-over distance

(c) Simplifying the problem by “merging” arrivals (especially in gradient zones) for a layered system

The interpreter errors are not quantifiable in a statistical sense. Also, the cross-over distance was defined on a trace-basis, i.e. no detailed interpolation between adjacent traces was made for a more accurate definition of this value (very time-consuming and for over 4000 shots, not practical) and only rounded to the nearest 5 m. Trace spacing is 12.5 m between hydrophone-channels along the streamer and it thus possible to create a jump in refractor depth by several meters by selecting the “wrong” nearest trace for the cross-over distance and apply the rounding as mentioned above. In an attempt to quantify this error, a 5% error bar was chosen in Figure 12 where the refractor-depth is correlated to the 3.5 kHz data. Moreover, the depth-conversion of the 3.5 kHz data is rather challenging given that velocities quickly increase with burial depth, ice content and the regional unconformity that reflects a yet unknown change in the velocity-depth profile.

Fatigue during the analysis may also play a role and therefore the task of picking was spread over different times in the day, interrupted by other tasks (to relax the eye and hand of the interpreter) and frequently double-checked and re-analysed. Only if consistent results were achieved between the initial and re-analysed values, the velocity values were “accepted”.

The near-seafloor geology of the submerged shelf is complicated for various reasons: only a thin cover of Holocene sedimentation, ice-scouring of the surface, high-velocity material from ice-bearing sediments within few meters of the seafloor, and a regional erosional unconformity. It is often possible that a thin veneer of soft sediments with a slow velocity that theoretically should generate a refraction (and practically does), is not detected in the MCS data as it is overwhelmed by the much faster arrival from the underlying either ice-bearing sediments or from the more consolidated sediments of the unconformity. If the top veneer is less than 4 meter thick, it is lost in the resolution of the MCS data (assuming a velocity of 1550 – 1600 m/s and a frequency of 80-90 Hz for the MCS data).

Overall, the study undertaken was not to calculate highly accurate velocity values, but to verify the general nature of velocity changes across the shelf edge and verify the earlier work by Pullan et al. (1987) and re-map the critical boundaries relative to the two threshold values of 1800 m/s (onset of ice-bearing sediments) and 2500 m/s (for continuous permafrost). It is recommended, that either the refraction statics tool is used more widely, or a more complete tomography static solution (e.g. following that of Ramachandran et al., 2011) is being conducted to obtain a more detailed velocity field. Both are currently outside the scope of the study presented here.

6 Conclusions

Based on the new analyses we can conclude that the major boundaries drawn by Pullan et al. (1987) are confirmed (despite the 30+ year difference in time of the analysis and even older vintage of the seismic data used in the earlier work). However, several additions were made to the occurrence of ice distribution in the sediments from the new data and near the edge of permafrost a shift to shallower data is warranted for the first occurrence of ice within the sediment. The boundary can be re-drawn and using the multi-beam data can be estimated to be just “south” of the zone of pingo-like-features (PLF) at the shelf edge.

The thresholds defined in the earlier study of 1800 m/s as indicator of some ice-content and 2500 m/s for some ice-bonded and discontinuous permafrost appear valid; however, it is suggested to collect core and make careful measurements of the P-wave velocity as function of ice content and re-justify the threshold that (at this point) appear arbitrary and not supported by measurements in the Pullan et al. (1987) study.

Regionally, the refraction work shows that the first refractor is (if not the seafloor itself) likely the underlying unconformity. Deeper and secondary refractions were also identified at several locations, but the shallow water and thus multiple-generation, creates multiple refractions and therefore a rather complex wave-front overlap at further offsets. It was also noted, that at some locations, the multiple creates clear low-velocity refractions from the seafloor that are completely overshadowed from faster, underlying sediments at the near-offset portion of the streamer and earlier arrival times. It may be possible to combine primary and multiple refractions for a more detailed near-seafloor velocity model, but this is outside the scope of the current study.

At selected locations the 3.5 kHz data were correlated to the MCS refraction results and a primary indicator for ice-occurrences was identified: brightening of the reflection surface and loss of acoustic penetration underneath. However, the regional unconformity may also be a reflection surface that can mimic this acoustic response (especially when combined with a change to a more sand-rich sediment environment) and gives the false impression of ice-content. Analysis of the 3.5 kHz data alone using acoustic penetration as ice-indicator is thus misleading.

References

Dallimore, S.R., Paull, C.K., Collett, T.S., Jin, Y.K., Mienert, J., Mangelsdorf, K., Riedel, M., 2012. Drilling to investigate methane release and geologic processes associated with warming permafrost and gas hydrate deposits beneath the Beaufort Sea Shelf. IODP Pre-Proposal 806, available online at http://iodp.org/

O'Regan, M., de Vernal, A., Hill, P., Hillaire-Marcel, C., Jakobsson, M., Moran, K., Rochon, A., St-Onge, G., 2010. Late quaternary paleoceanography and glacial dynamics in the Beaufort Sea, IODP pre-proposal #753, available online at http://iodp.org/.

Pullan, S., MacAulay, M.H., Hunter, J.A.M., Good, R.I., Gagne, R.M., Burns, R.A., 1987. Permafrost distribution determined from seismic refraction, in: Marine Science Atlas of the Beaufort Sea: Geology and Geophysics, ed. by B.R. Pelletier, Geological Survey of Canada Miscellaneous Report 40.

Ramachandran, K., Bellefleur, G., Brent, T., Riedel, M., Dallimore, S.R., 2011. Imaging Permafrost Velocity Structure Using High Resolution 3D Seismic Tomography, Geophysics 76, B187 (2011); doi:10.1190/geo2010-0353.1

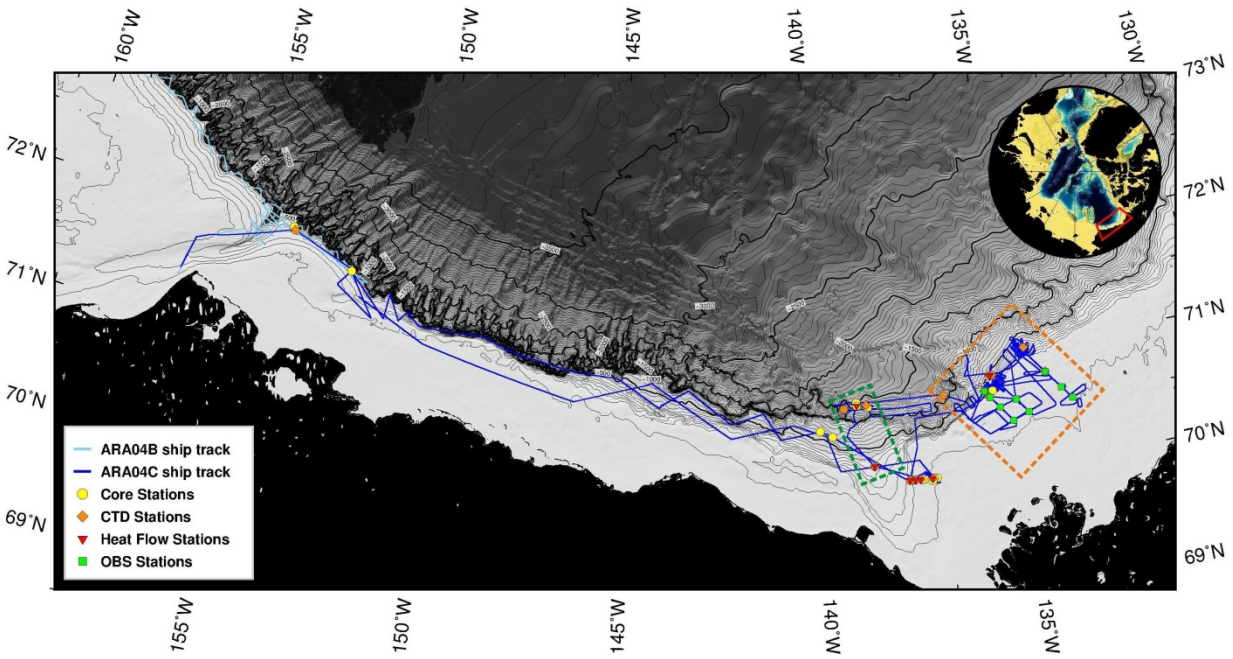

Figure 1. Overview map of the ship track for Expedition ARA04C. The expedition is split into two parts: September 6 - 9, 2013 in Alaskan waters off Barrow, and September 10 – 24, 2013 in Canadian waters off the Mackenzie Delta shelf and slope region. The small green box defines the region for IODP pre-proposals 753 (O'Regan et al., 2010) and the orange box defines the research region for IODP pre-proposal 806 (Dallimore et al., 2012).

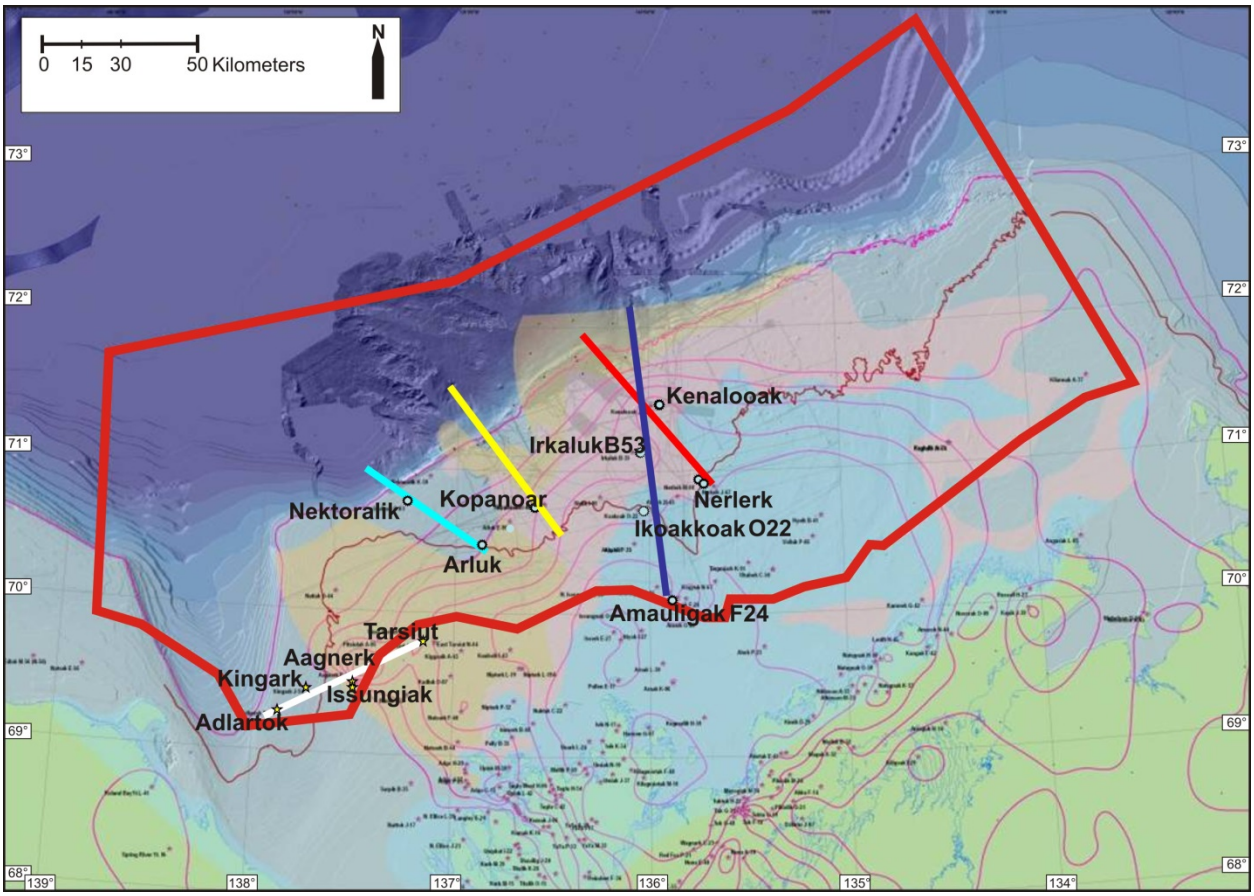

Figure 2. Location map of five main transects selected for regional characterization of permafrost distribution based on selected industry well sites. In order of priority, the transects are "red", "yellow" "blue", "cyan", and "white". The map shows in red the outline of the area of the permit for Expedition ARA04C, regions of permafrost occurrences after Pullan et al. (1987). Contour-lines are defining depth of permafrost as determined from temperature data acquired at industry well sites. The 100 m isobaths line is shown in pink, and the 50 m isobaths line (southern limit of permit for using the 1200 in^3 airgun array) is shown in brown.

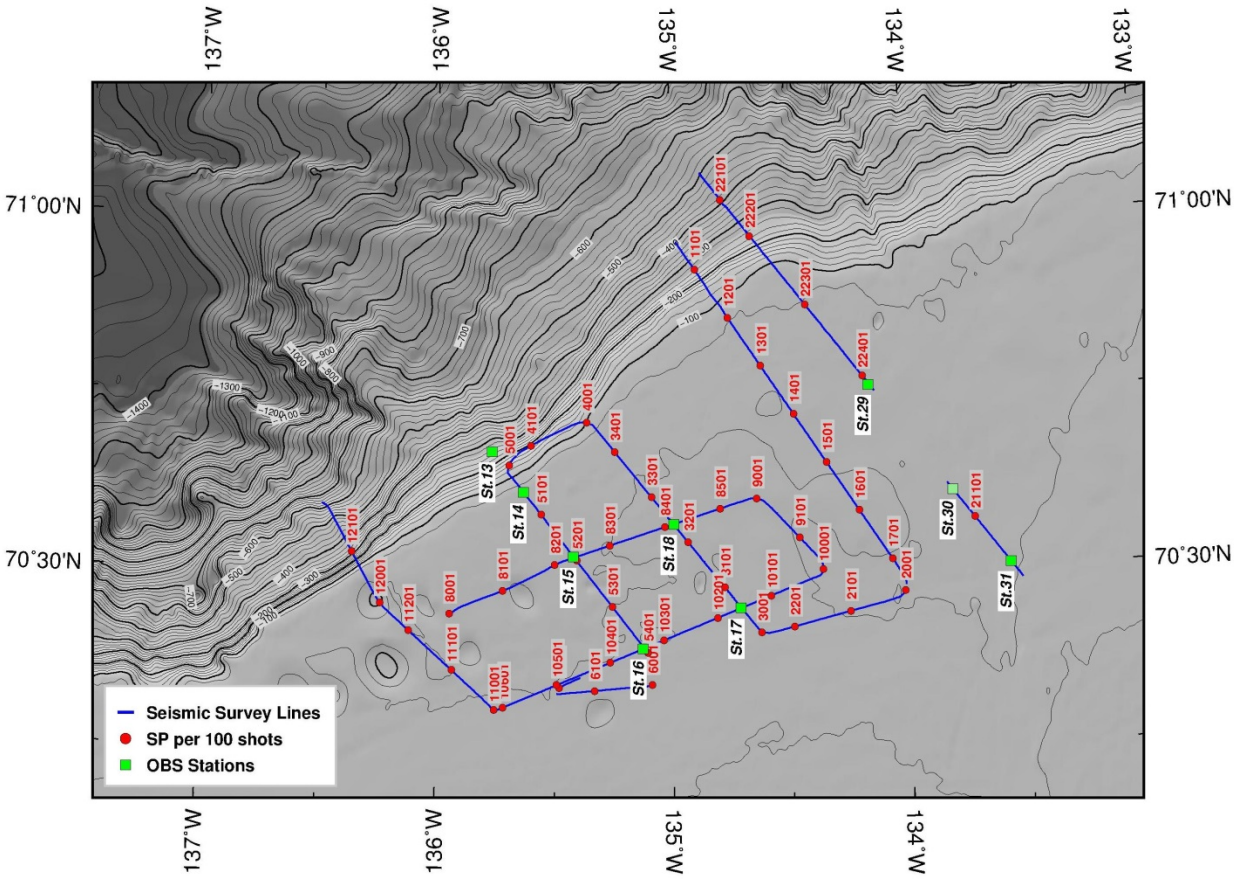

Figure 3. Track-chart showing seismic survey lines (blue) of Expedition ARA04C. Labels for shot-numbers are in red. Green symbols are locations of the ocean bottom seismometers.

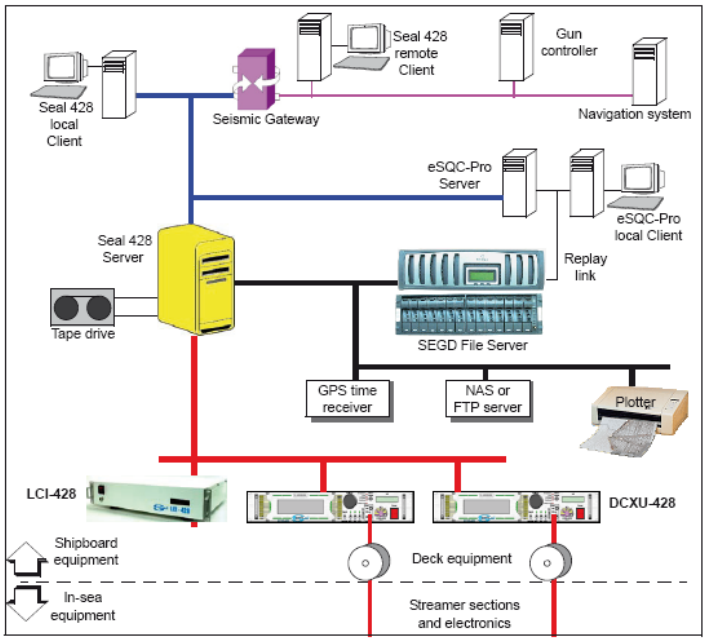

Figure 4. Schematic diagram of the multi-channel seismic system on Araon.

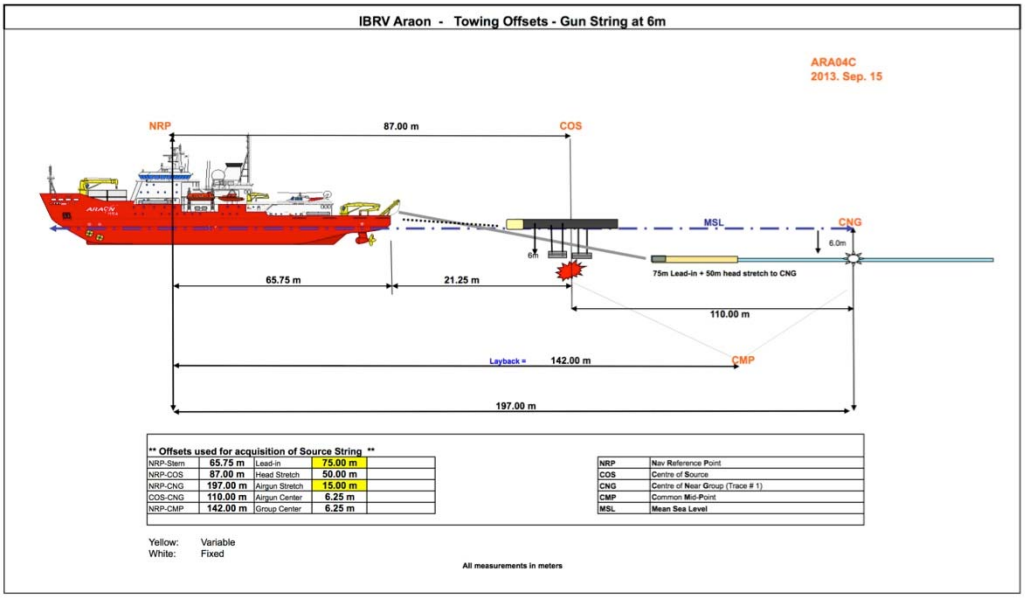

Figure 5. Geometry and offset information for the seismic survey conducted during Expedition ARA04C.

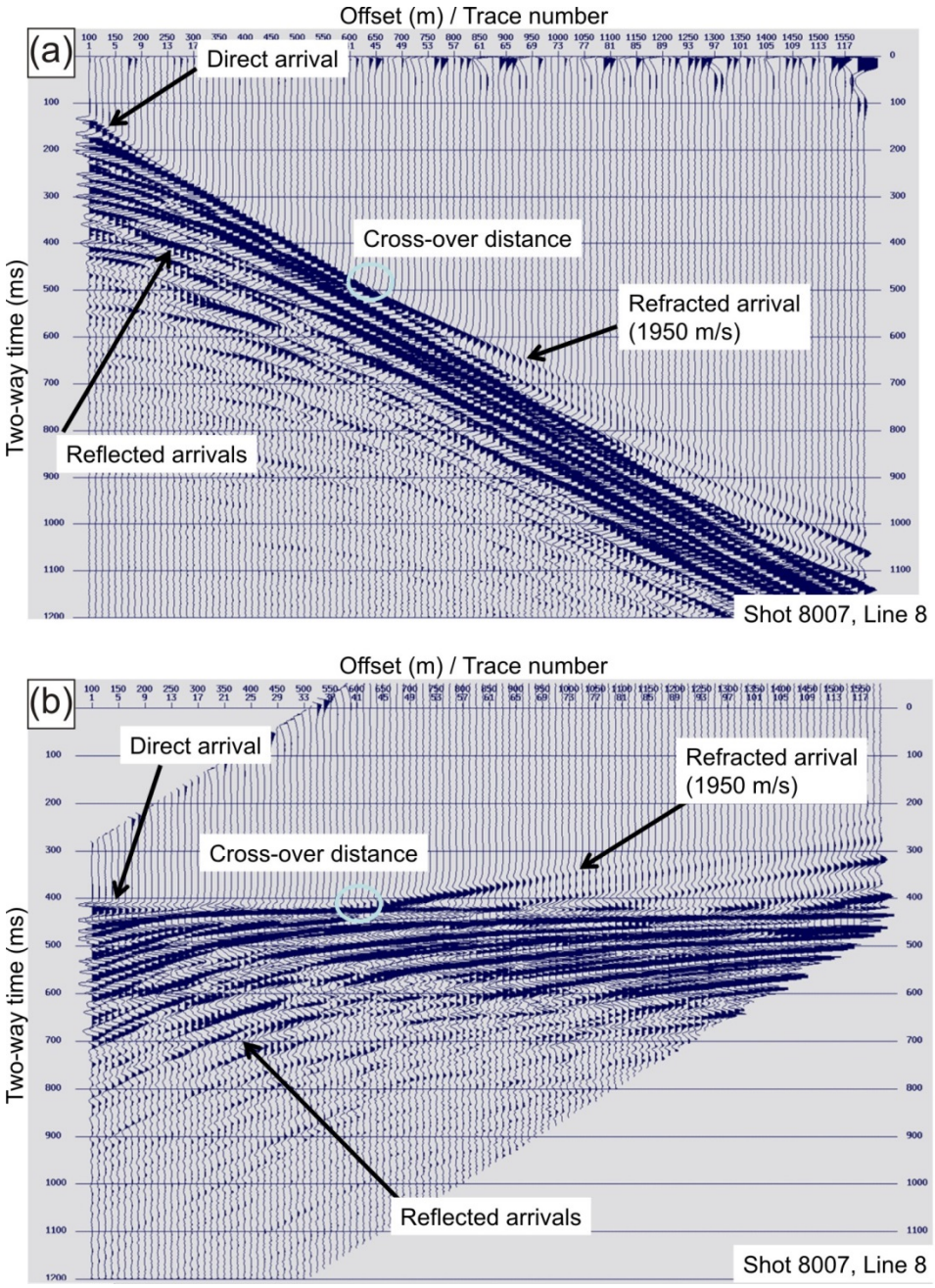

Figure 6. Example Shot gather (shot 8007) from Line 8, identifying arrivals and geometrical parameters used to define refraction velocity: (a) regular shot gather, and (b) shot gather reduced by the velocity of water (1450 m/s).

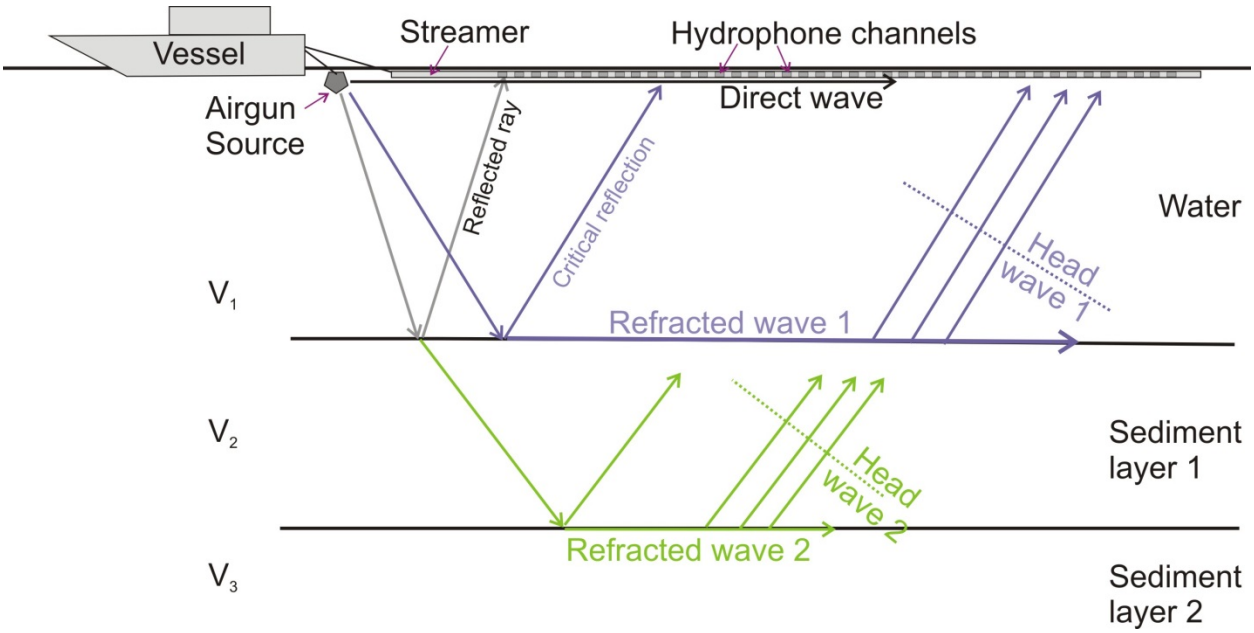

Figure 7. Generation of refracted waves at interfaces between two layers, where the velocity of the underlying medium is higher than the velocity in the upper medium. Shown in this figure is a marine case of water over two sedimentary layers and generation of two head-waves at the corresponding interfaces.

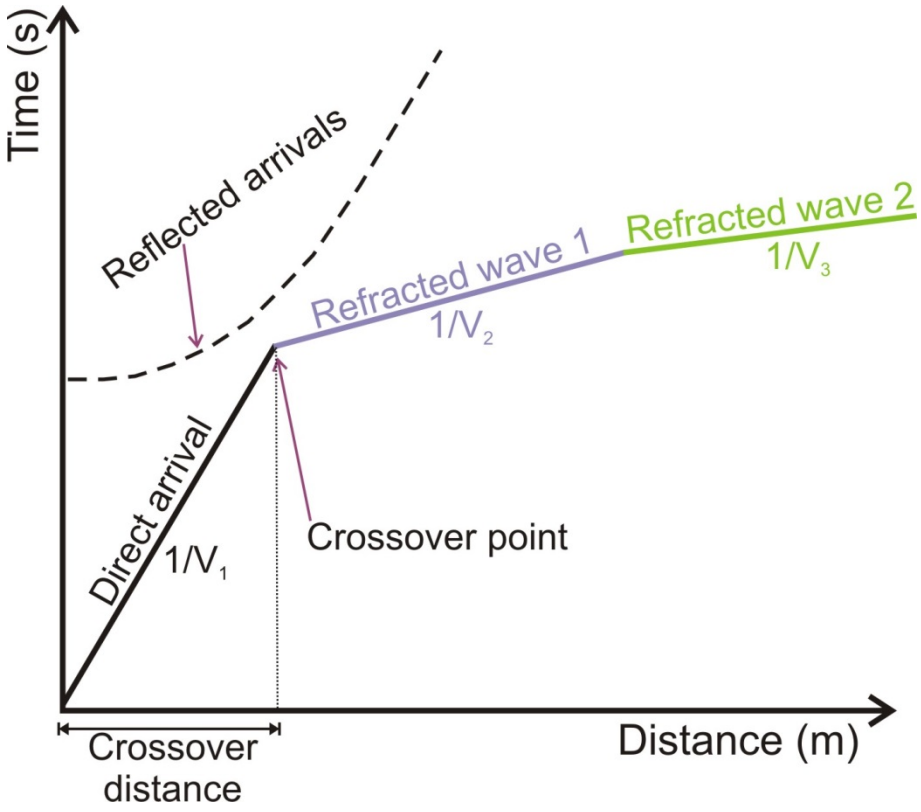

Figure 8. Schematic shot gather showing required parameters to define seismic velocity (V) and depth of refractor (crossover distance). The slopes of the linear arrivals for the directed, and refracted waves is the slowness (inverse of velocity) of that layer.

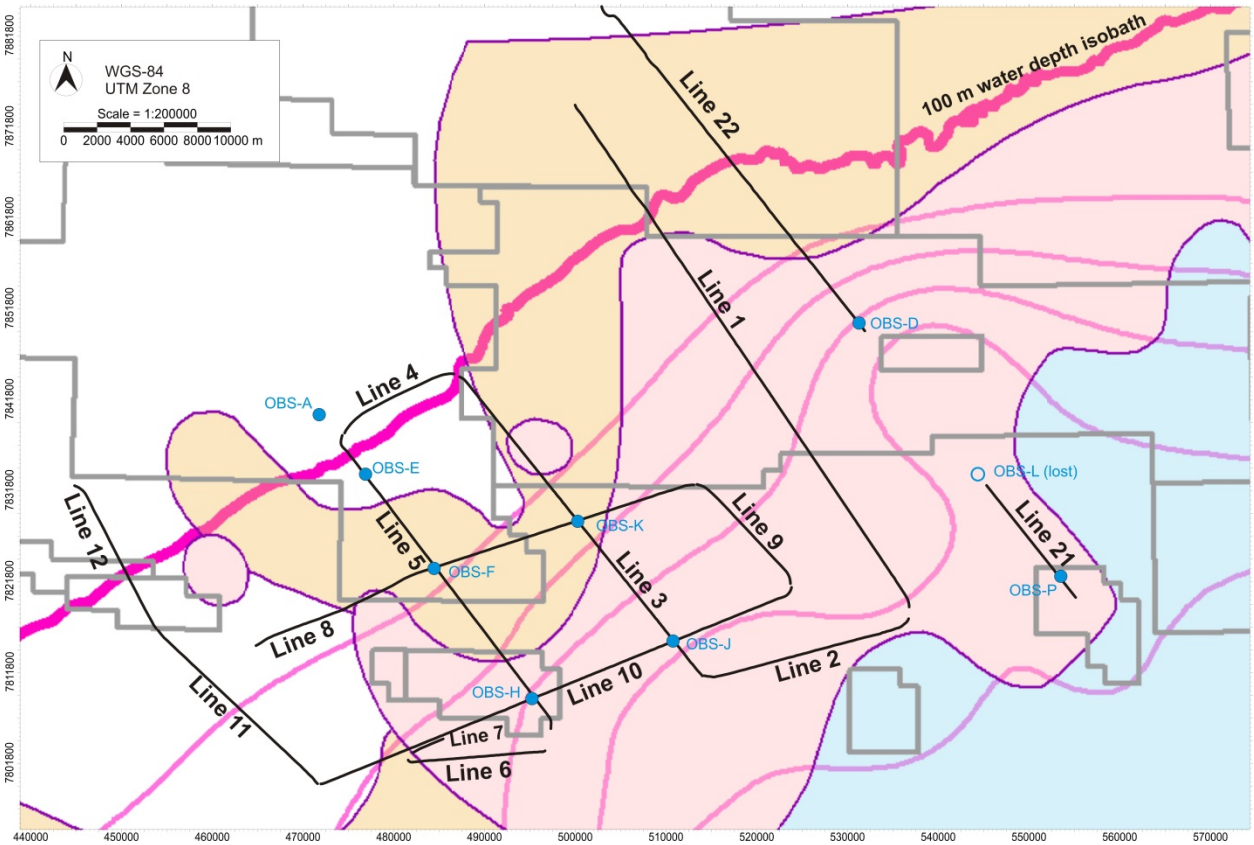

Figure 9a. Map showing locations of seismic lines from Expedition ARA04C overlain on the map of permafrost distribution by Pullan et al. (1987).

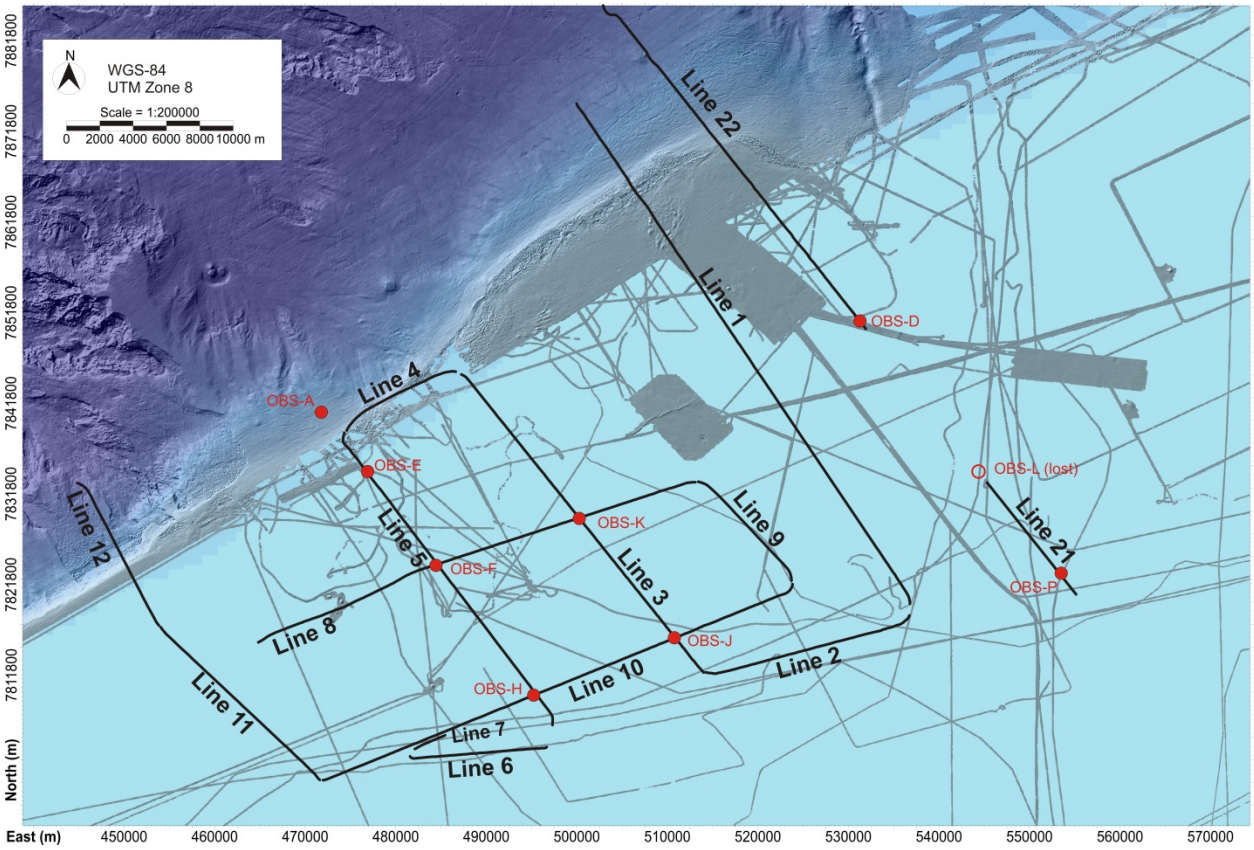

Figure 9b. Map showing locations of seismic lines from Expedition ARA04C overlain on multi-beam bathymetry.

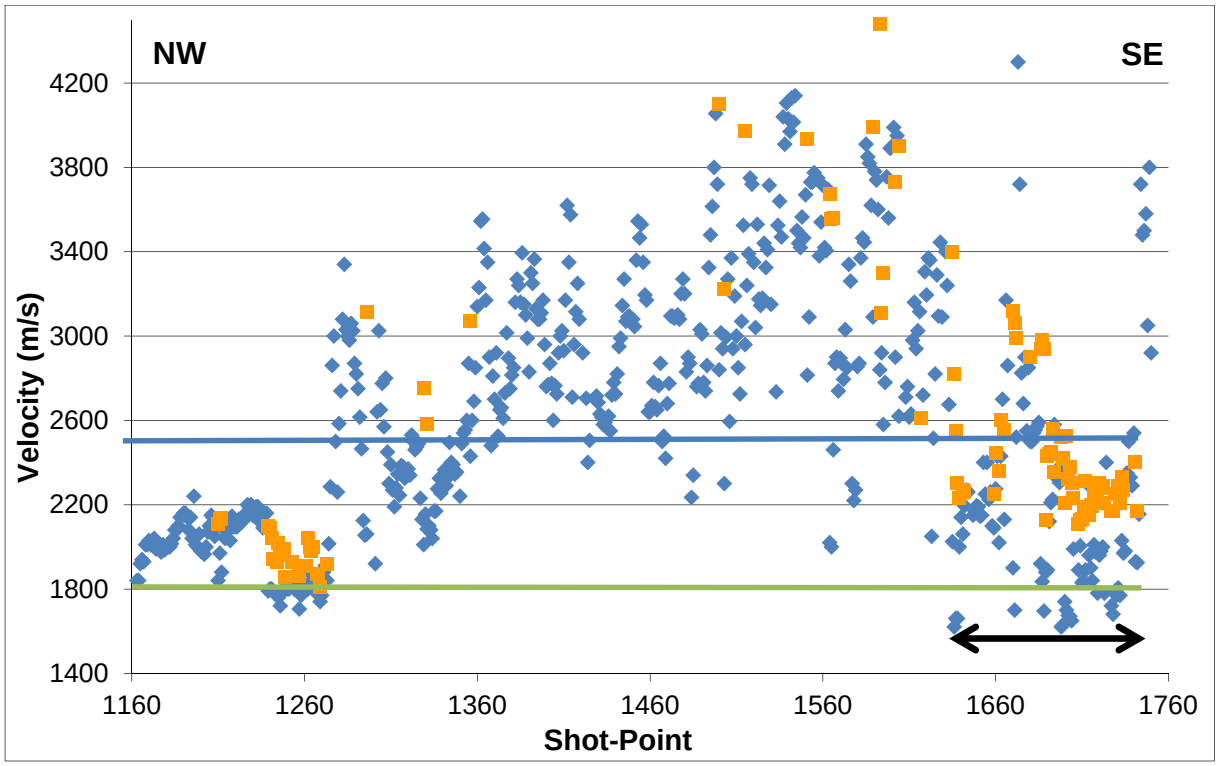

Figure 10a. Results of refraction velocity analysis (hand-picked) from Line-1 of Expedition ARA04C. Shot-numbers increase from NW to SE. Velocity from the first refractor (blue diamonds) and second refractor (orange squares) are shown together with the 1800 m/s threshold (solid green line) and the threshold of 2500 m/s (blue solid line) used by Pullan et al. (1987) as indicator for ice-bearing sediments and zones of continuous permafrost, respectively. The black arrow indicates the extent where Line-1 crosses the sediment-filled Kugmallit-Trough.

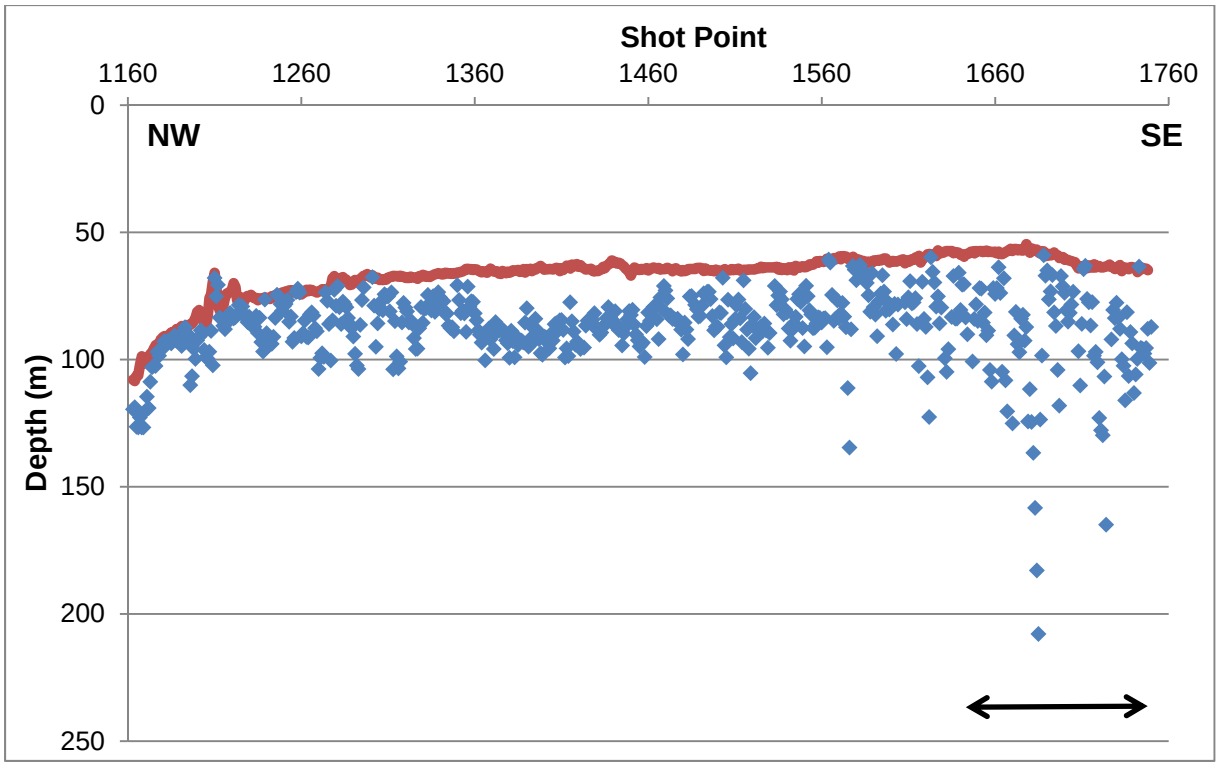

Figure 10b. Results of refraction analysis along Line-1 of Expedition ARA04C showing depth of first refraction in meter below sea-surface (blue diamonds) and seafloor determined from MCS data (dark red line). The black arrow indicates the extent where Line-1 crosses the sediment-filled Kugmallit-Trough. Shot-numbers increase from NW to SE.

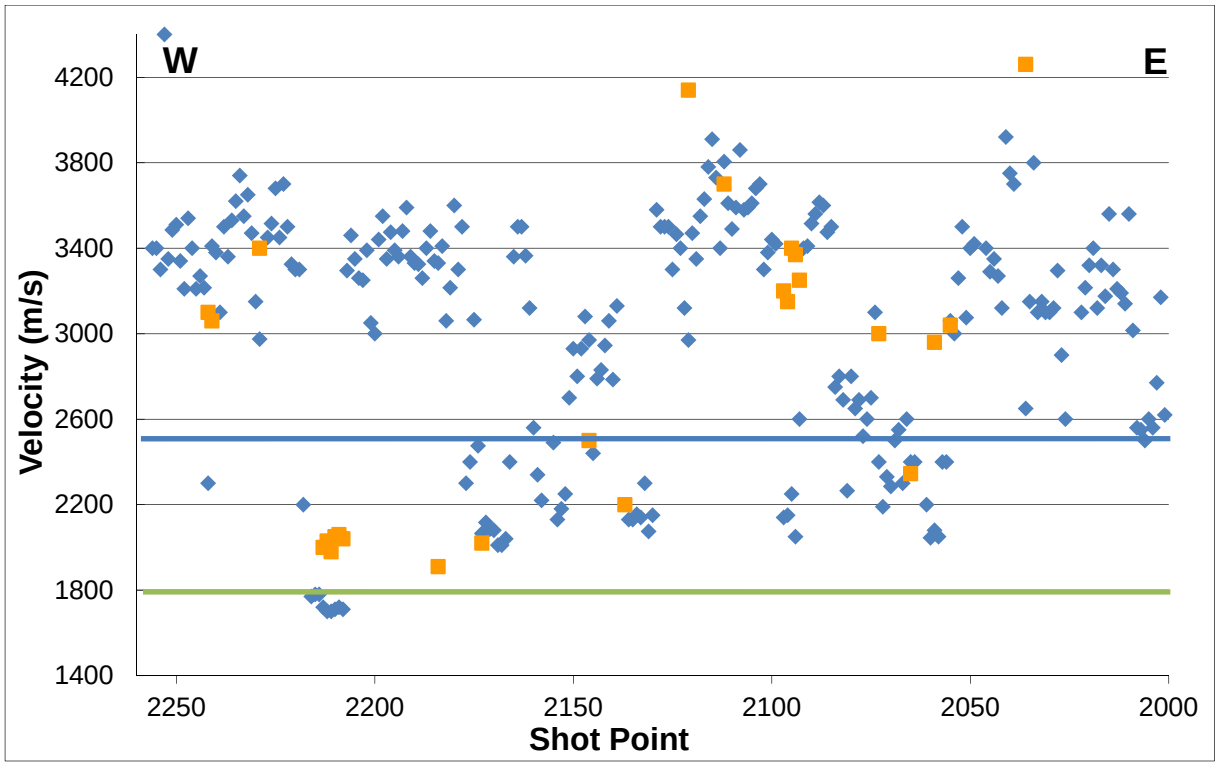

Figure 10c. Results of refraction velocity analysis (hand-picked) from Line-2 of Expedition ARA04C. Velocity from the first refractor (blue diamonds) and second refractor (orange squares) are shown together with the 1800 m/s threshold (solid green line) and the threshold of 2500 m/s (blue solid line) used by Pullan et al. (1987) as indicator for ice-bearing sediments and zones of continuous permafrost, respectively. Shot-numbers increase from E to W.

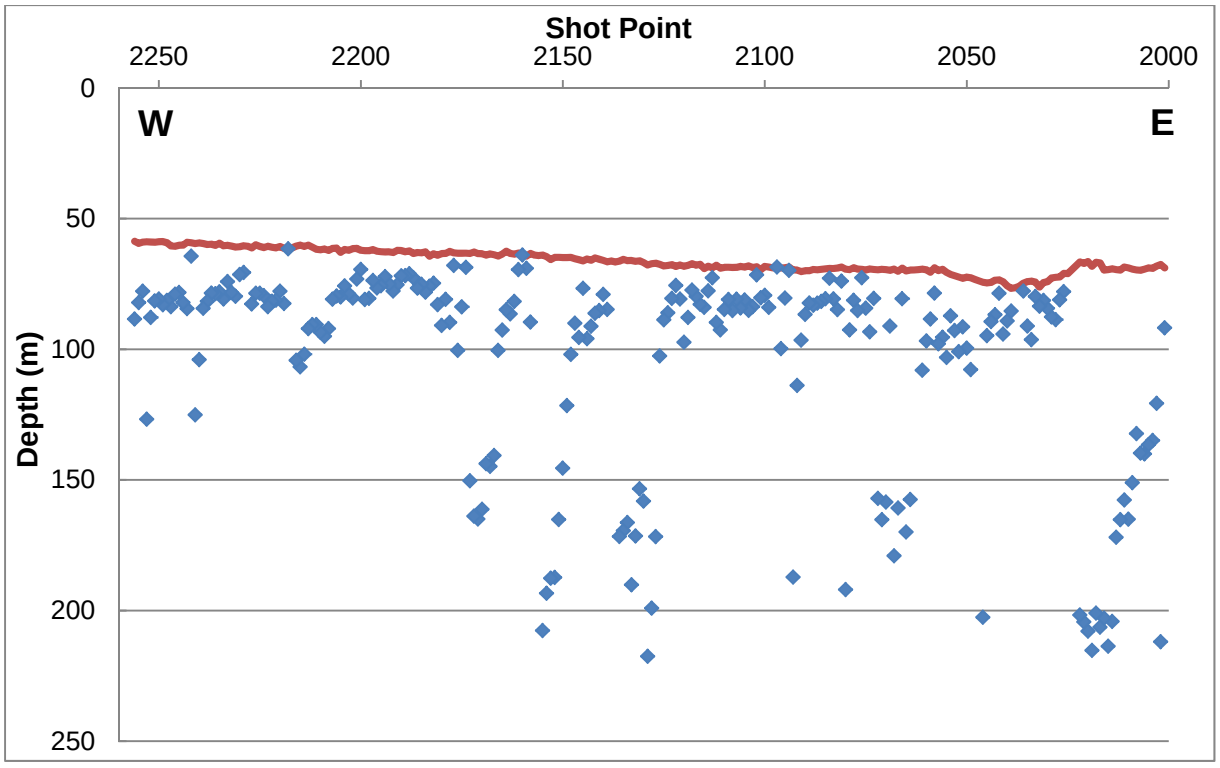

Figure 10d. Results of refraction analysis along Line-2 of Expedition ARA04C showing depth of first refraction in meter below sea-surface (blue diamonds) and seafloor determined from MCS data (dark red line). Shot-numbers increase from E to W.

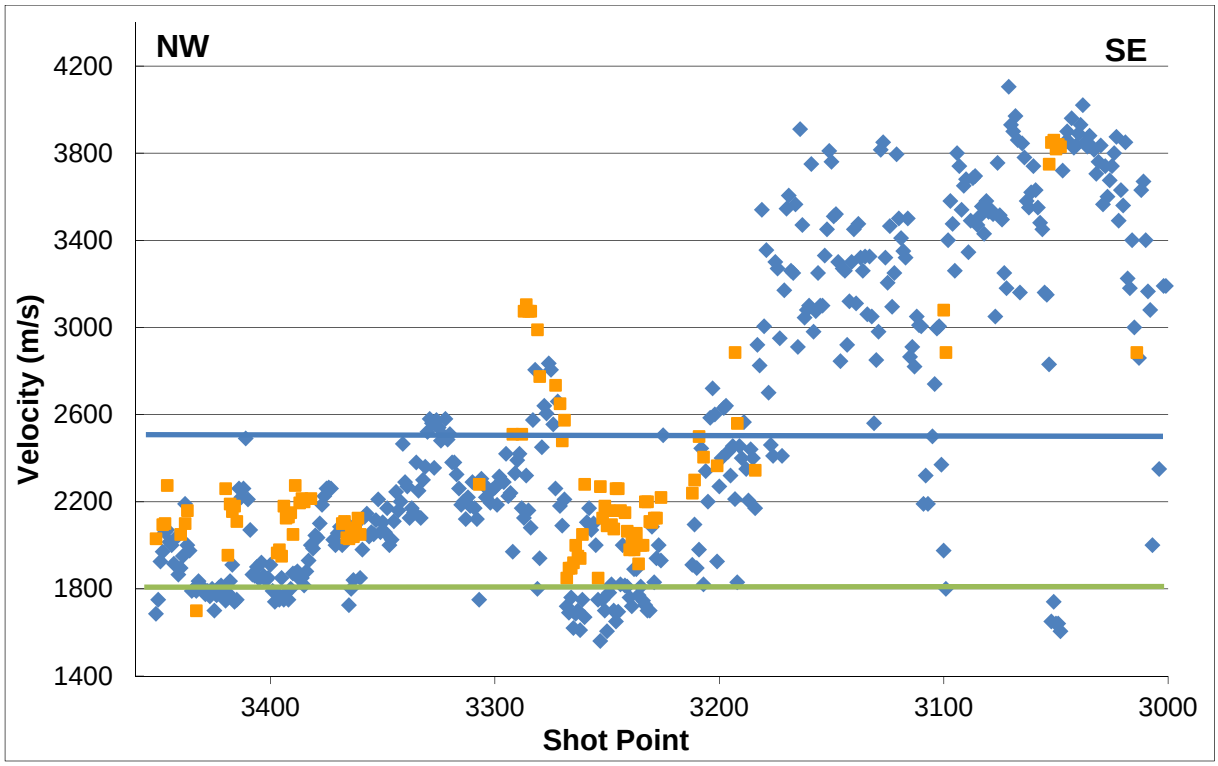

Figure 10e. Results of refraction velocity analysis (hand-picked) from Line-3 of Expedition ARA04C. Velocity from the first refractor (blue diamonds) and second refractor (orange squares) are shown together with the 1800 m/s threshold (solid green line) and the threshold of 2500 m/s (blue solid line) used by Pullan et al. (1987) as indicator for ice-bearing sediments and zones of continuous permafrost, respectively. Shot-numbers increase from SE to NW.

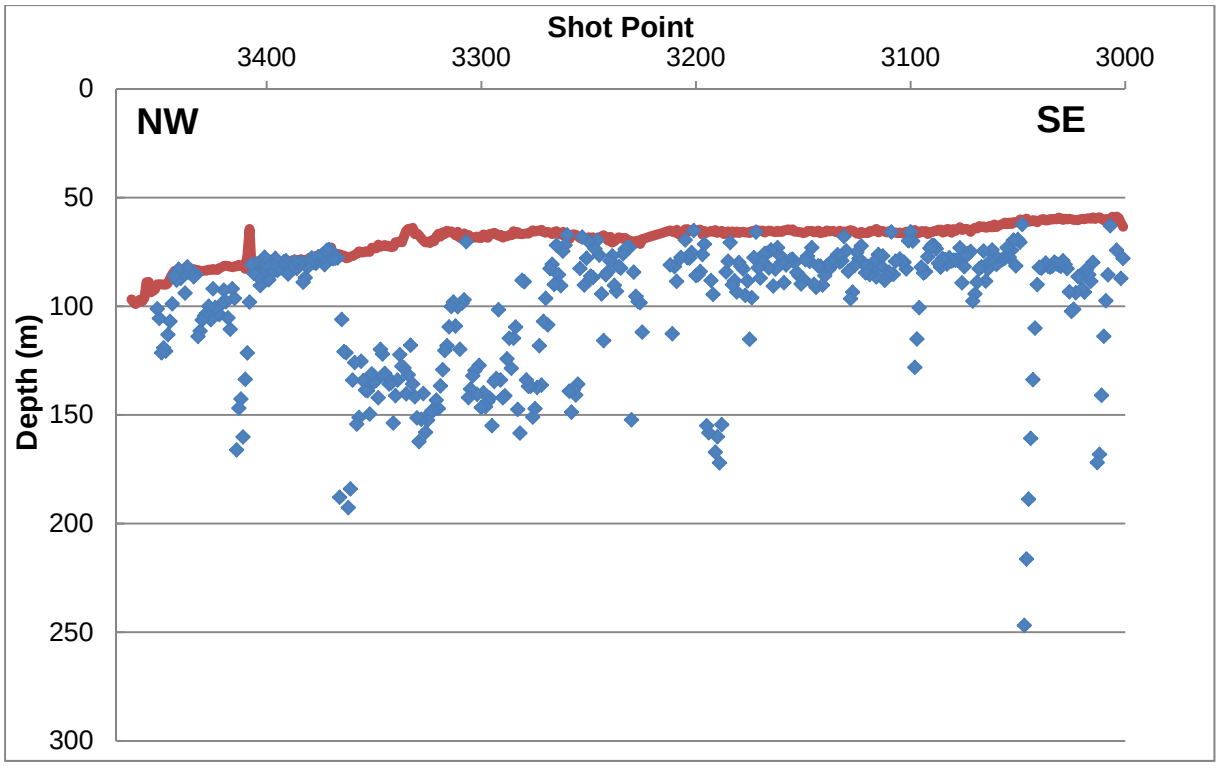

Figure 10f. Results of refraction analysis along Line-3 of Expedition ARA04C showing depth of first refraction in meter below sea-surface (blue diamonds) and seafloor determined from MCS data (dark red line). Shot-numbers increase from SE to NW. Refractions occurring from a depth above the seafloor are within the PLF-zone and 3D or topographic effects from dipping layers may cause this discrepancy.

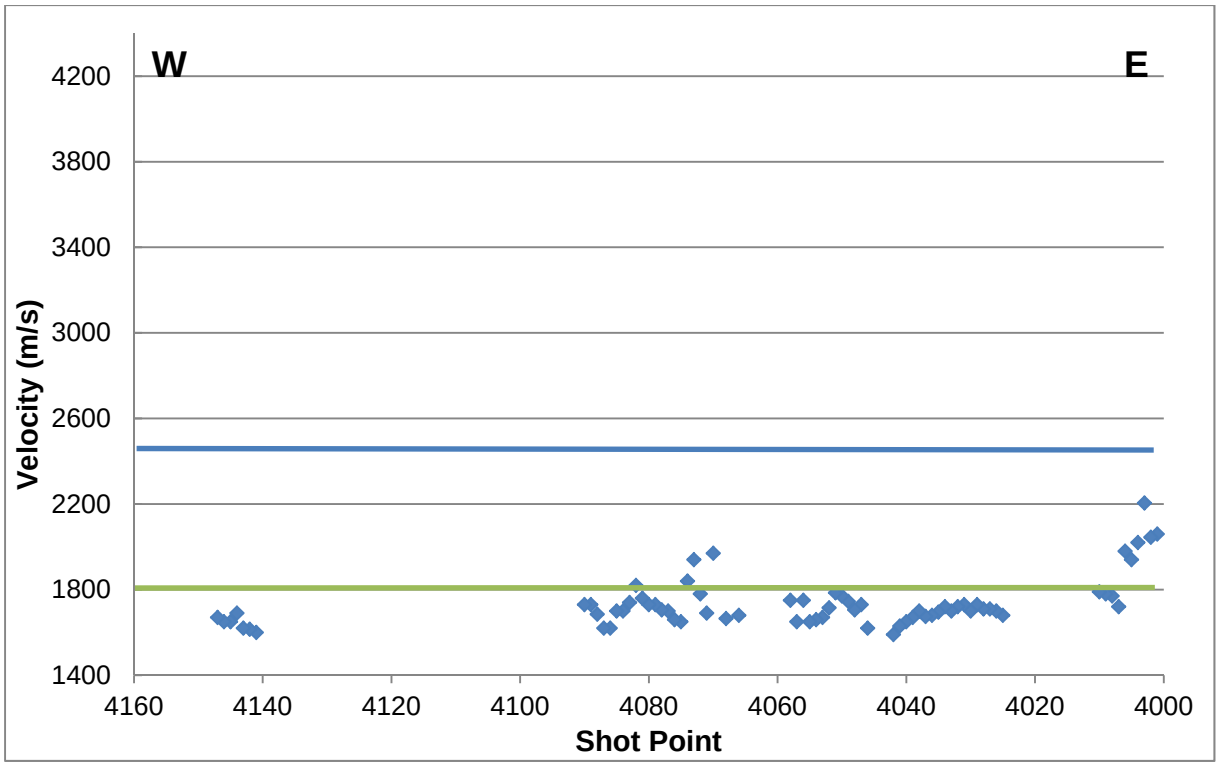

Figure 10g. Results of refraction velocity analysis (hand-picked) from Line-4 of Expedition ARA04C. Many gaps from no airgun shots as well as no detectable refractors exist along this line in addition to in-interpretable data at start and end of line (turns and non-flat streamer), which was shot "ad-hoc" parallel to the shelf edge to avoid ice that was seen at the end of Line-3 further to the North. Velocity from the first refractor (blue diamonds) are shown together with the 1800 m/s threshold (solid green line) and the threshold of 2500 m/s (blue solid line) used by Pullan et al. (1987) as indicator for ice-bearing sediments and zones of continuous permafrost, respectively. Shot-numbers increase from E to W.

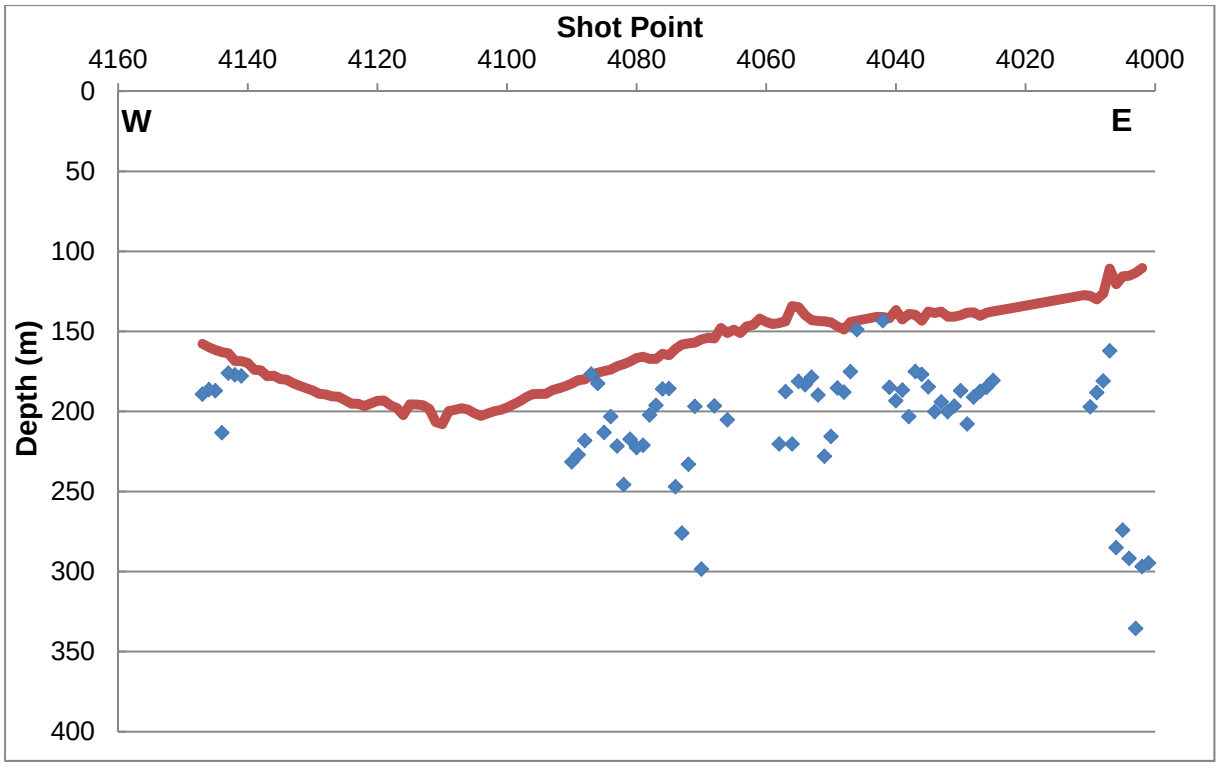

Figure 10h. Results of refraction analysis along Line-4 of Expedition ARA04C showing depth of first refraction in meter below sea-surface (blue diamonds) and seafloor determined from MCS data (dark red line). Shot-numbers increase from SE to NW. Refractions occurring from a depth above the seafloor are within the PLF-zone and 3D or topographic effects from dipping layers may cause this discrepancy.

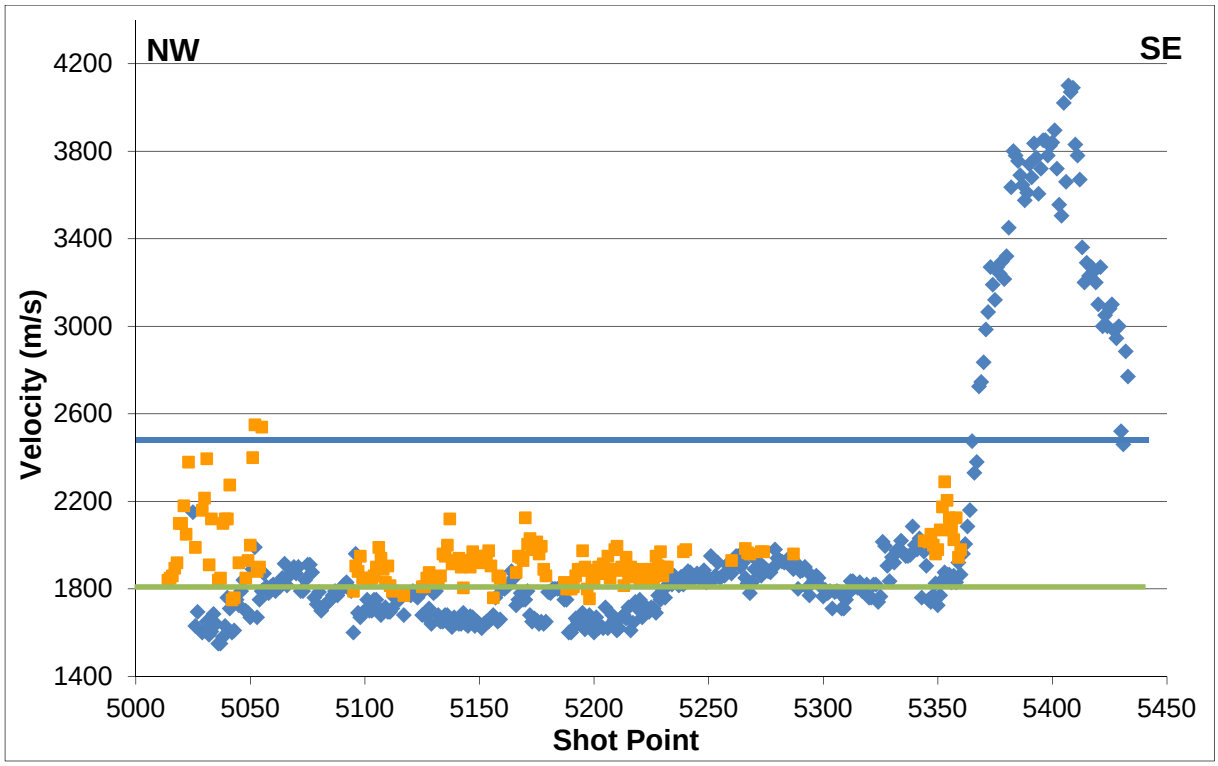

Figure 10i. Results of refraction velocity analysis (hand-picked) from Line-5 of Expedition ARA04C. Velocity from the first refractor (blue diamonds) and second refractor (orange squares) are shown together with the 1800 m/s threshold (solid green line) and the threshold of 2500 m/s (blue solid line) used by Pullan et al. (1987) as indicator for ice-bearing sediments and zones of continuous permafrost, respectively. Shot-numbers increase from NW to SE.

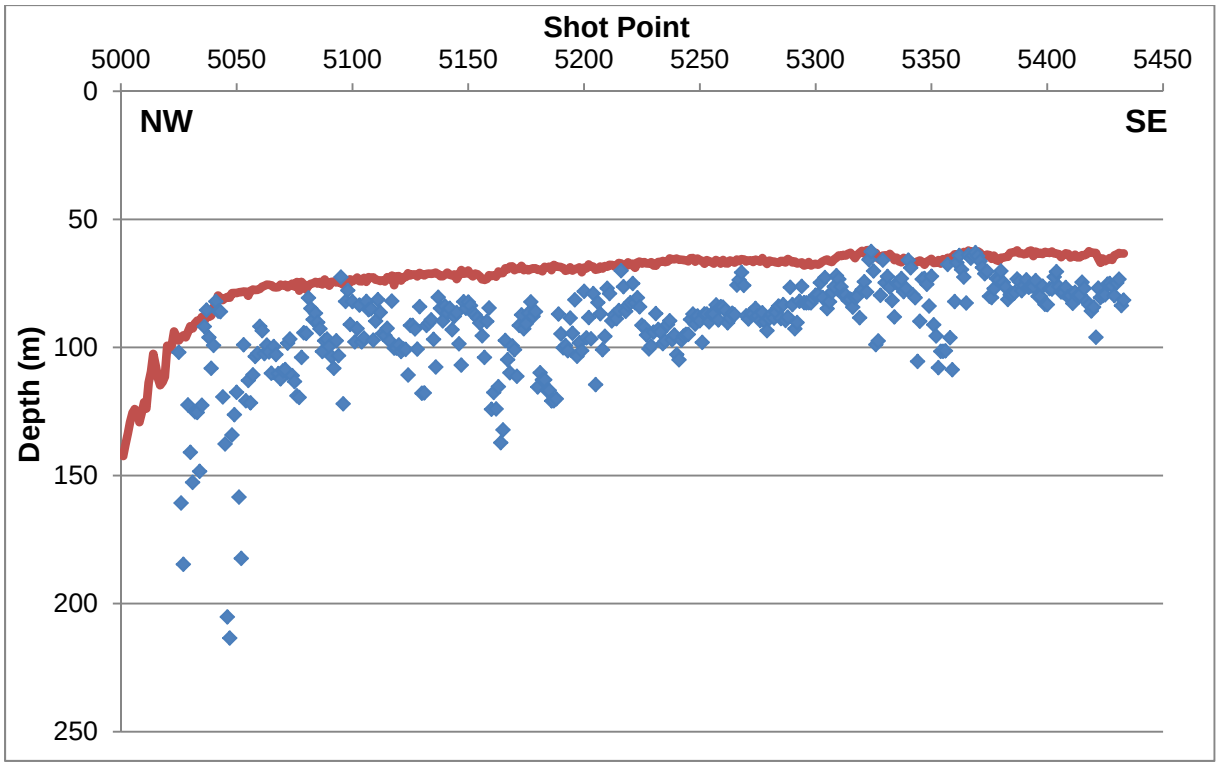

Figure 10j. Results of refraction analysis along Line-5 of Expedition ARA04C showing depth of first refraction in meter below sea-surface (blue diamonds) and seafloor determined from MCS data (dark red line). Shot-numbers increase from NW to SE.

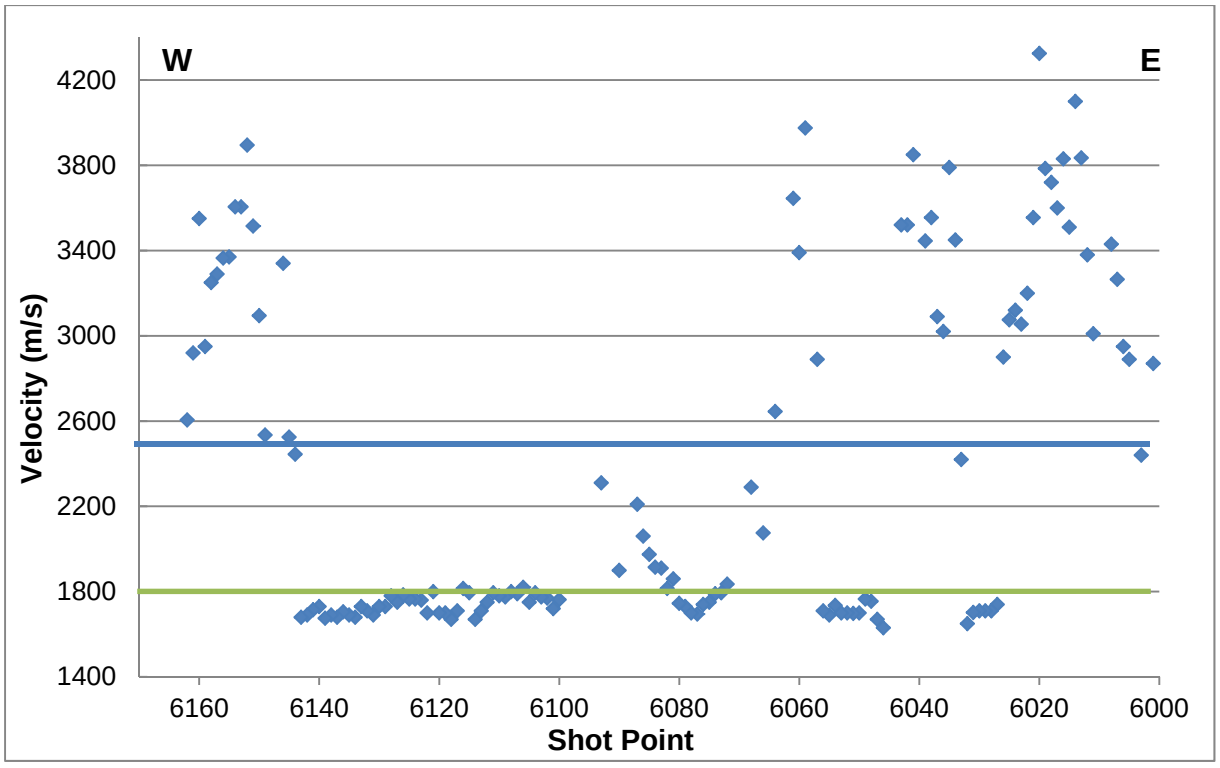

Figure 10k. Results of refraction velocity analysis (hand-picked) from Line-6 of Expedition ARA04C. Velocity from the first refractor (blue diamonds) is shown together with the 1800 m/s threshold (solid green line) and the threshold of 2500 m/s (blue solid line) used by Pullan et al. (1987) as indicator for ice-bearing sediments and zones of continuous permafrost, respectively. Shot-numbers increase from E to W.

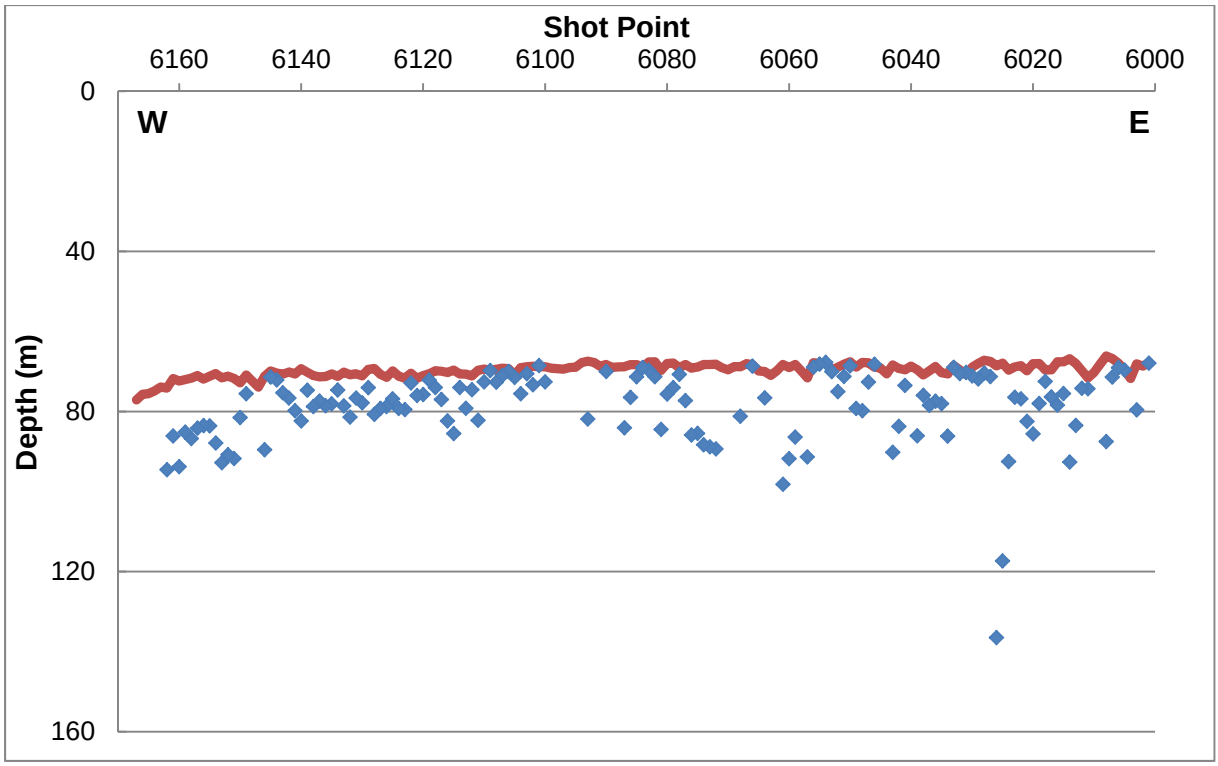

Figure 10l. Results of refraction analysis along Line-6 of Expedition ARA04C showing depth of first refraction in meter below sea-surface (blue diamonds) and seafloor determined from MCS data (dark red line). Shot-numbers increase from E to W.

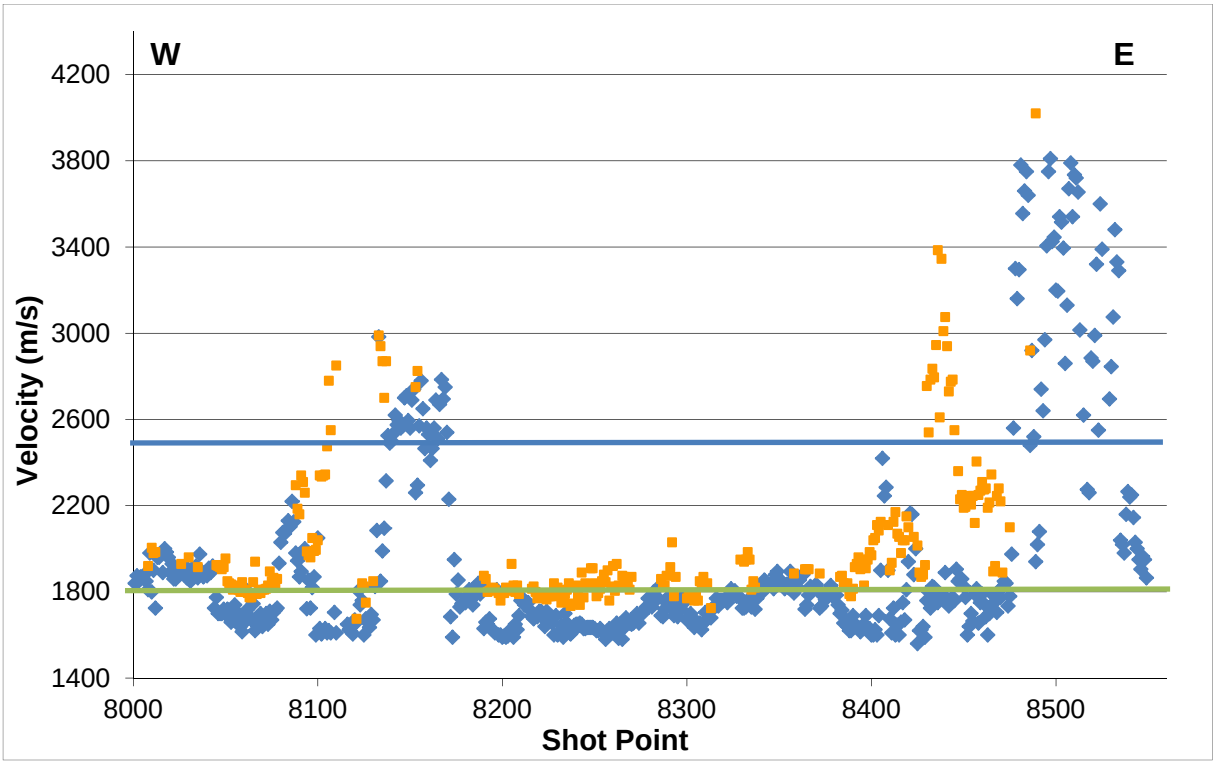

Figure 10m. Results of refraction velocity analysis (hand-picked) from Line-8 of Expedition ARA04C. Velocity from the first refractor (blue diamonds) and second refractor (orange squares) are shown together with the 1800 m/s threshold (solid green line) and the threshold of 2500 m/s (blue solid line) used by Pullan et al. (1987) as indicator for ice-bearing sediments and zones of continuous permafrost, respectively. Shot-numbers increase from W to E.

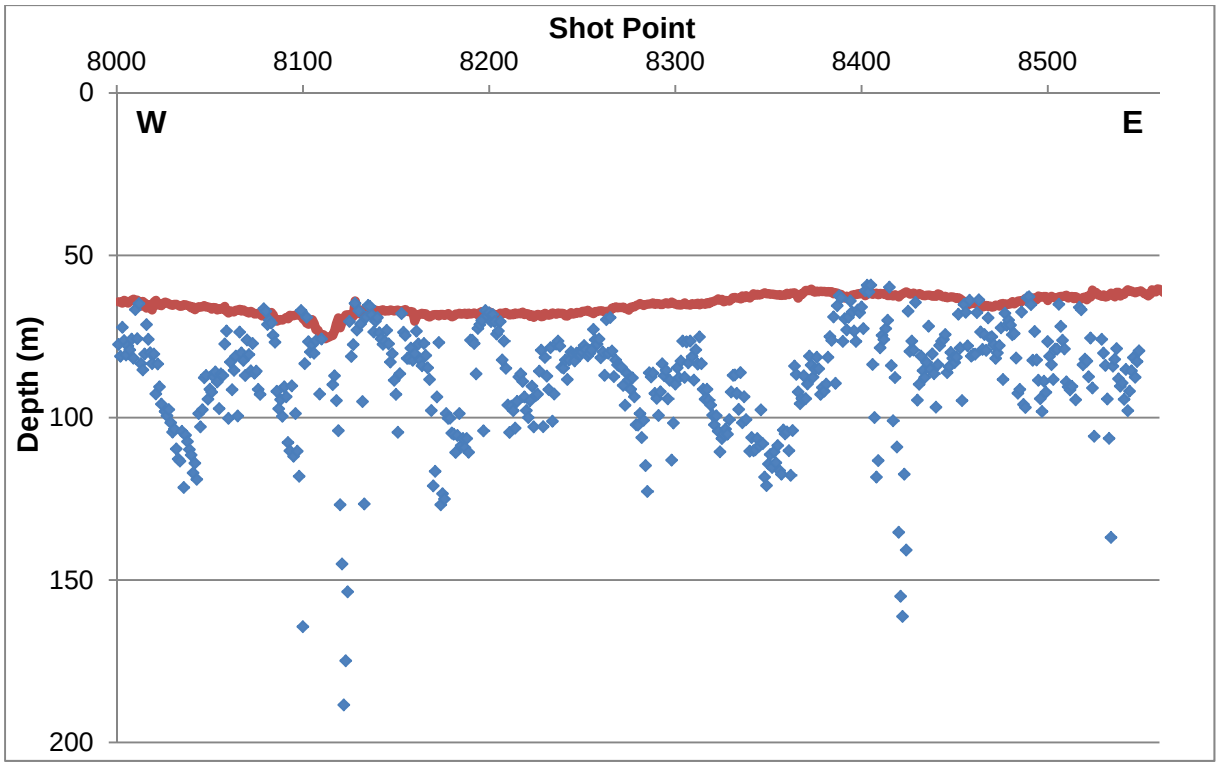

Figure 10n. Results of refraction analysis along Line-8 of Expedition ARA04C showing depth of first refraction in meter below sea-surface (blue diamonds) and seafloor determined from MCS data (dark red line). Shot-numbers increase from W to E.

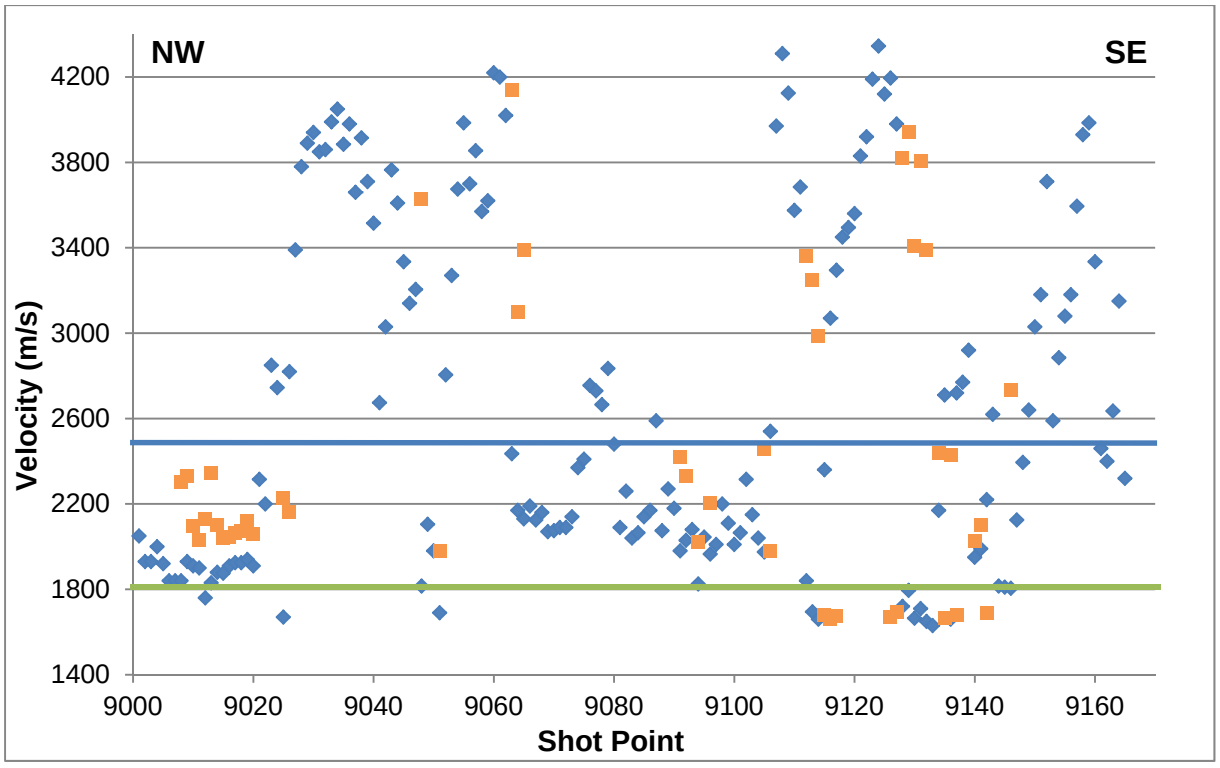

Figure 10o. Results of refraction velocity analysis (hand-picked) from Line-9 of Expedition ARA04C. Velocity from the first refractor (blue diamonds) and second refractor (orange squares) are shown together with the 1800 m/s threshold (solid green line) and the threshold of 2500 m/s (blue solid line) used by Pullan et al. (1987) as indicator for ice-bearing sediments and zones of continuous permafrost, respectively. Shot-numbers increase from NW to SE.

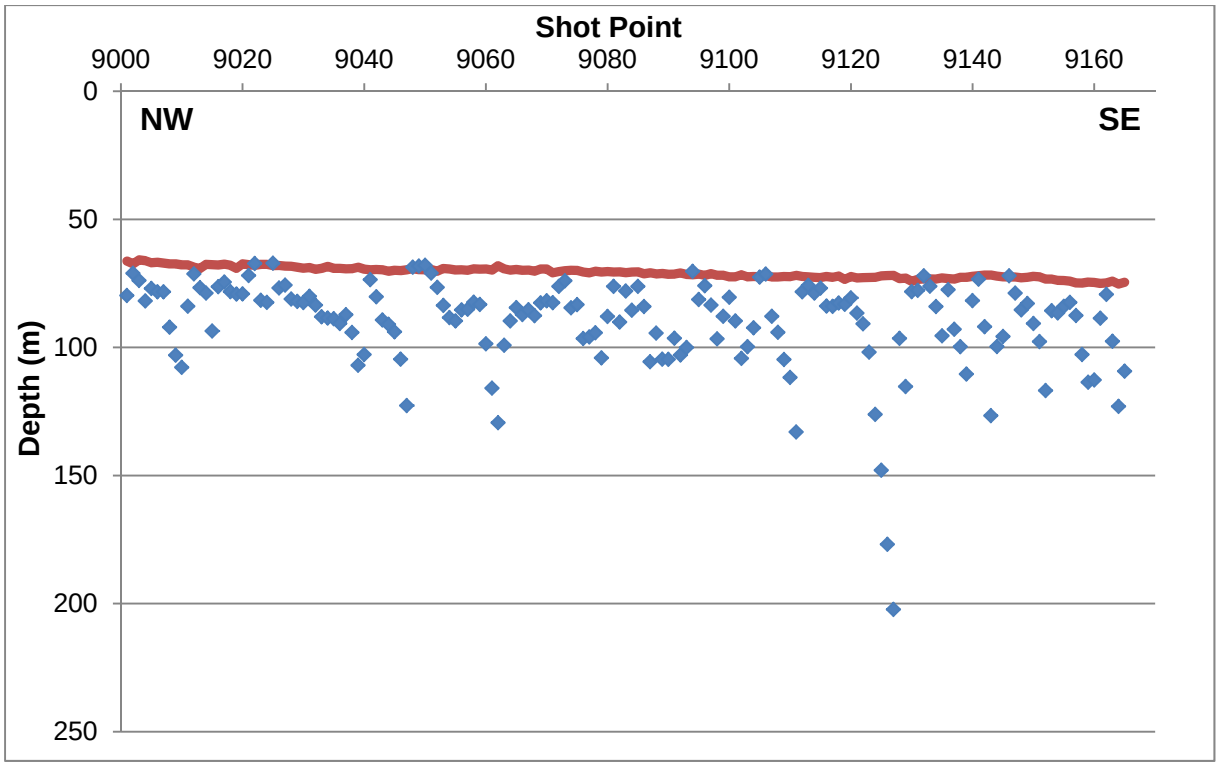

Figure 10p. Results of refraction analysis along Line-9 of Expedition ARA04C showing depth of first refraction in meter below sea-surface (blue diamonds) and seafloor determined from MCS data (dark red line). Shot-numbers increase from NW to SE.

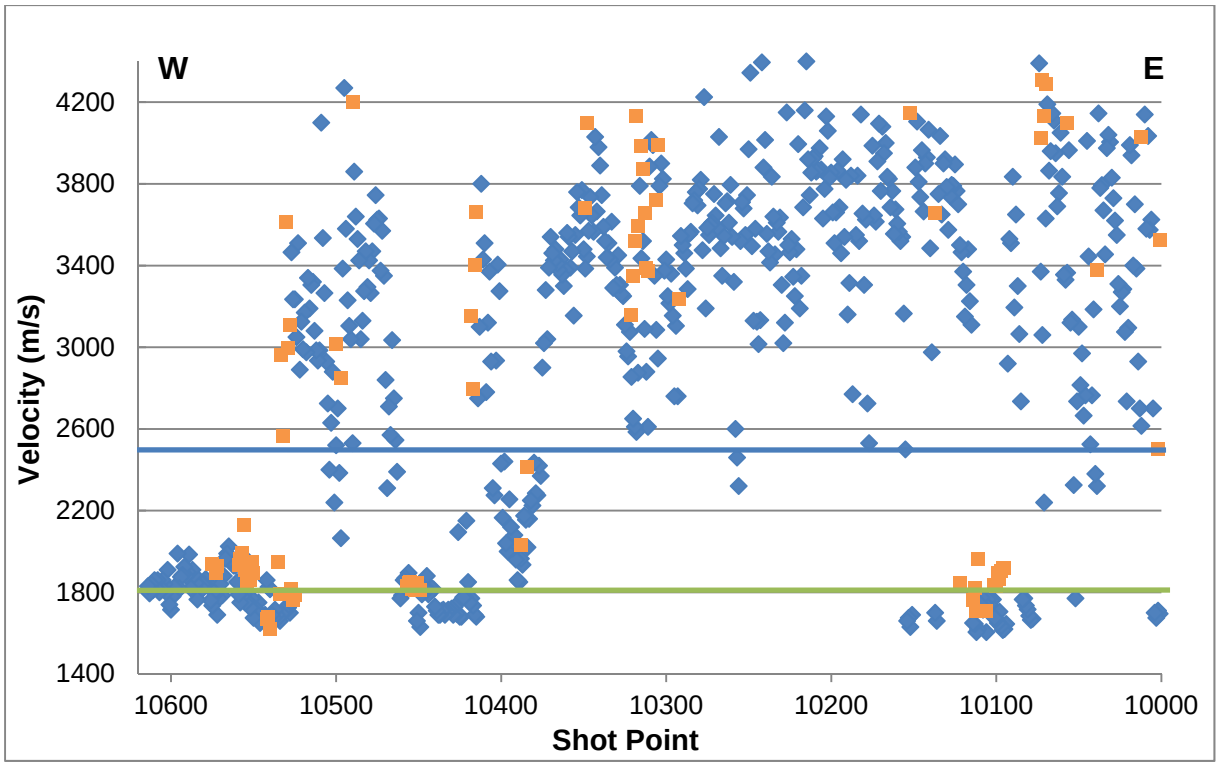

Figure 10q. Results of refraction velocity analysis (hand-picked) from Line-10 of Expedition ARA04C. Velocity only from the first refractor (blue diamonds) are shown together with the 1800 m/s threshold (solid green line) and the threshold of 2500 m/s (blue solid line) used by Pullan et al. (1987) as indicator for ice-bearing sediments and zones of continuous permafrost, respectively. Shot-numbers increase from E to W.

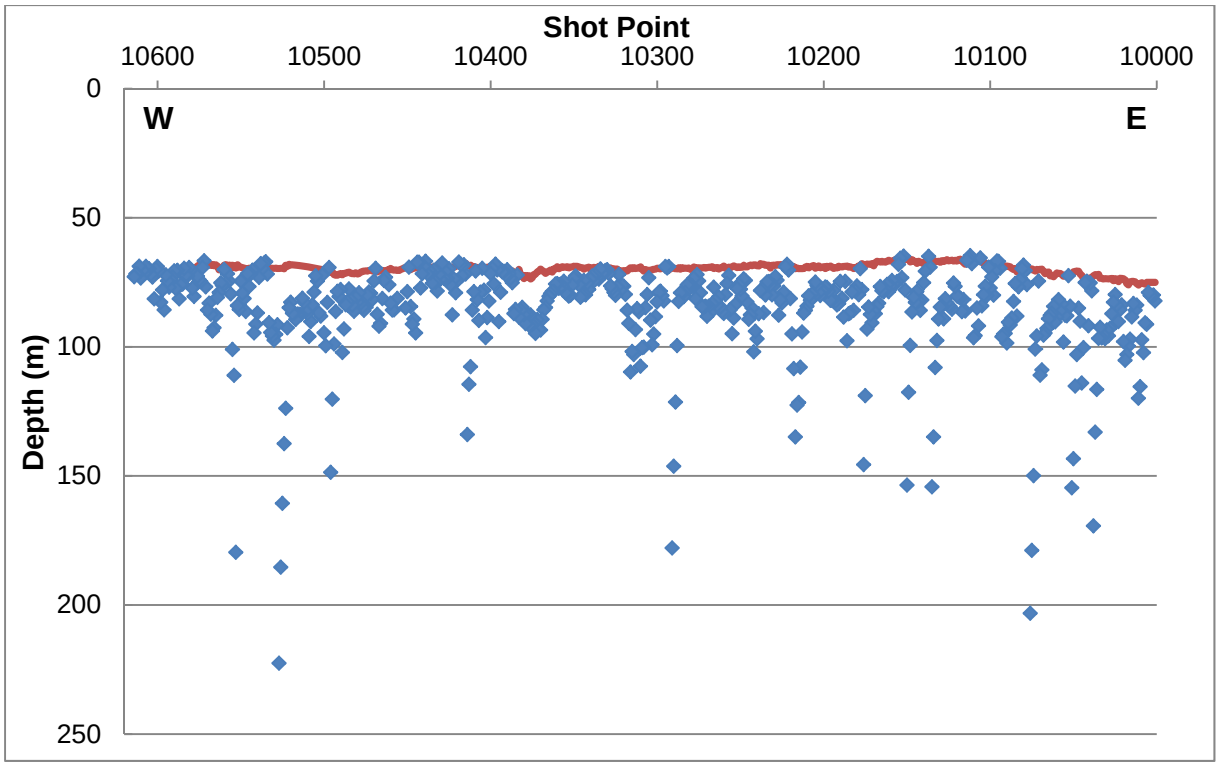

Figure 10r. Results of refraction analysis along Line-10 of Expedition ARA04C showing depth of first refraction in meter below sea-surface (blue diamonds) and seafloor determined from MCS data (dark red line). Shot-numbers increase from E to W.

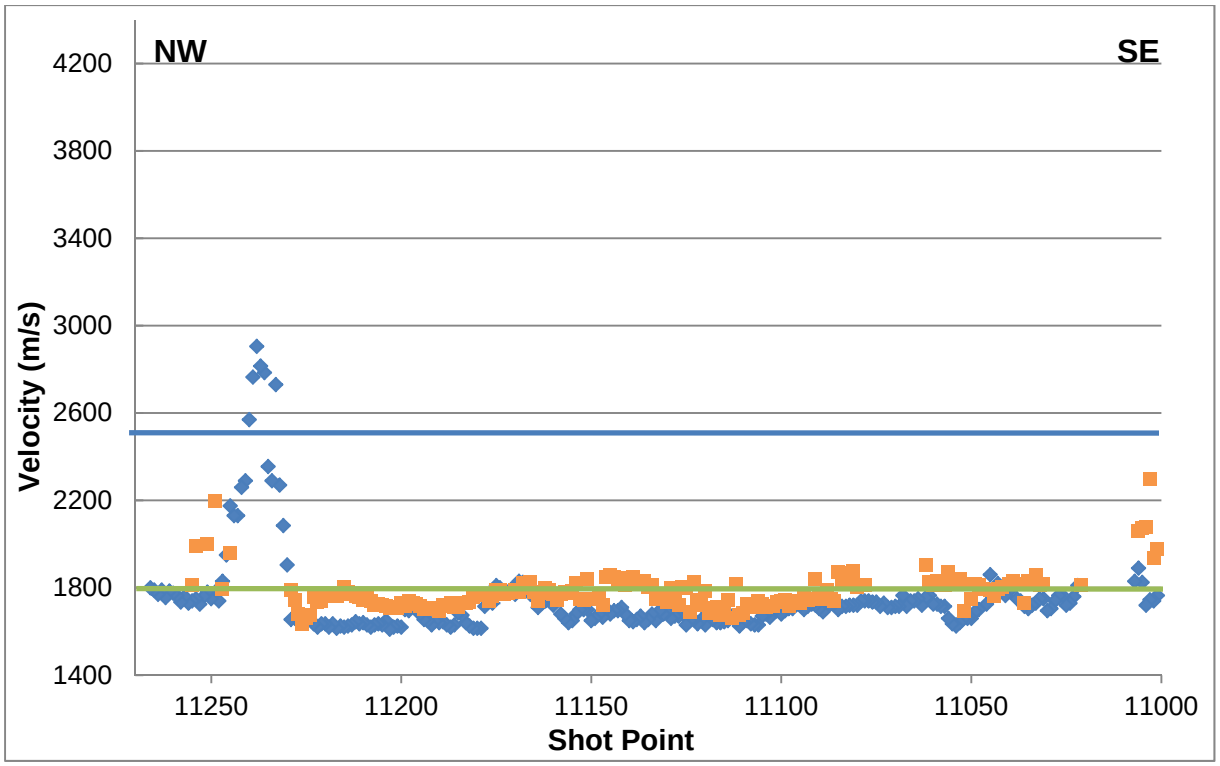

Figure 10s. Results of refraction velocity analysis (hand-picked) from Line-11 of Expedition ARA04C. Velocity only from the first refractor (blue diamonds) are shown together with the 1800 m/s threshold (solid green line) and the threshold of 2500 m/s (blue solid line) used by Pullan et al. (1987) as indicator for ice-bearing sediments and zones of continuous permafrost, respectively. Shot-numbers increase from SE to NW.

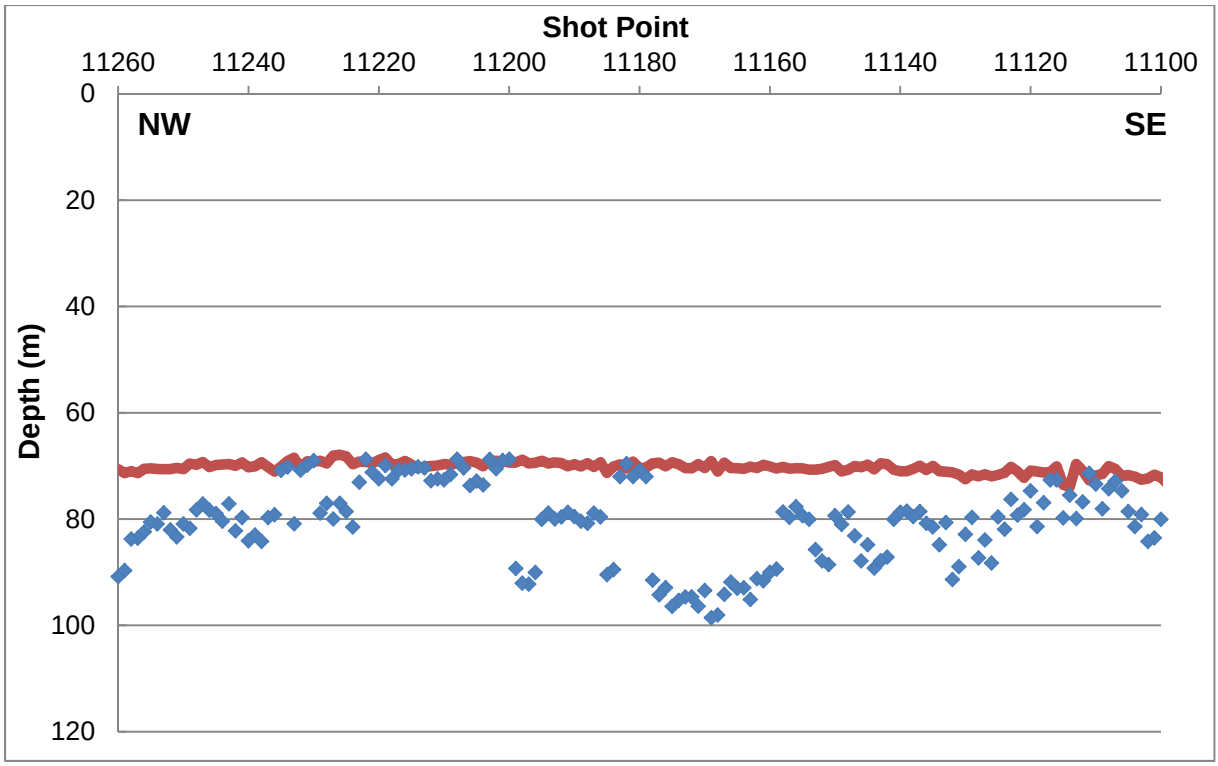

Figure 10t. Results of refraction analysis along Line-11 of Expedition ARA04C showing depth of first refraction in meter below sea-surface (blue diamonds) and seafloor determined from MCS data (dark red line). Shot-numbers increase from SE to NW.

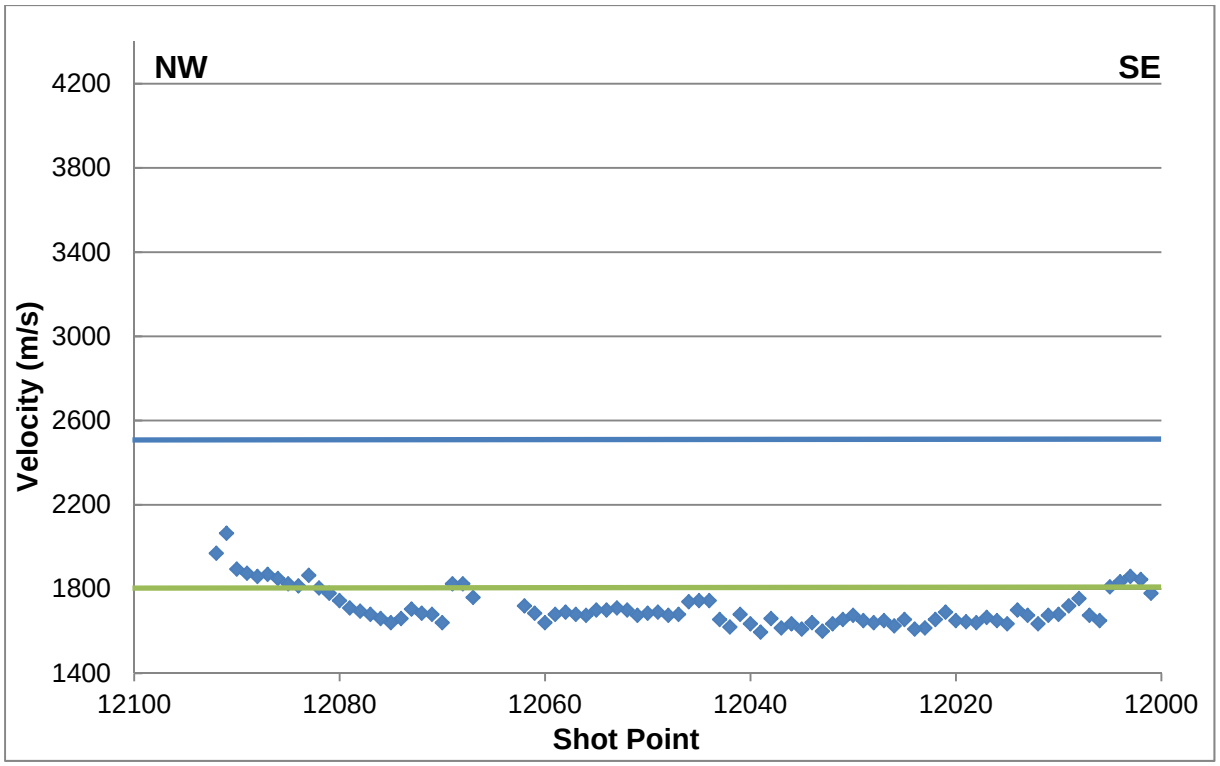

Figure 10u. Results of refraction velocity analysis (hand-picked) from Line-12 of Expedition ARA04C. Velocity only from the first refractor (blue diamonds) are shown together with the 1800 m/s threshold (solid green line) and the threshold of 2500 m/s (blue solid line) used by Pullan et al. (1987) as indicator for ice-bearing sediments and zones of continuous permafrost, respectively. Shot-numbers increase from SE to NW. Note: The steep slopes towards the end of the line (see next image) create apparent velocities that are too high.

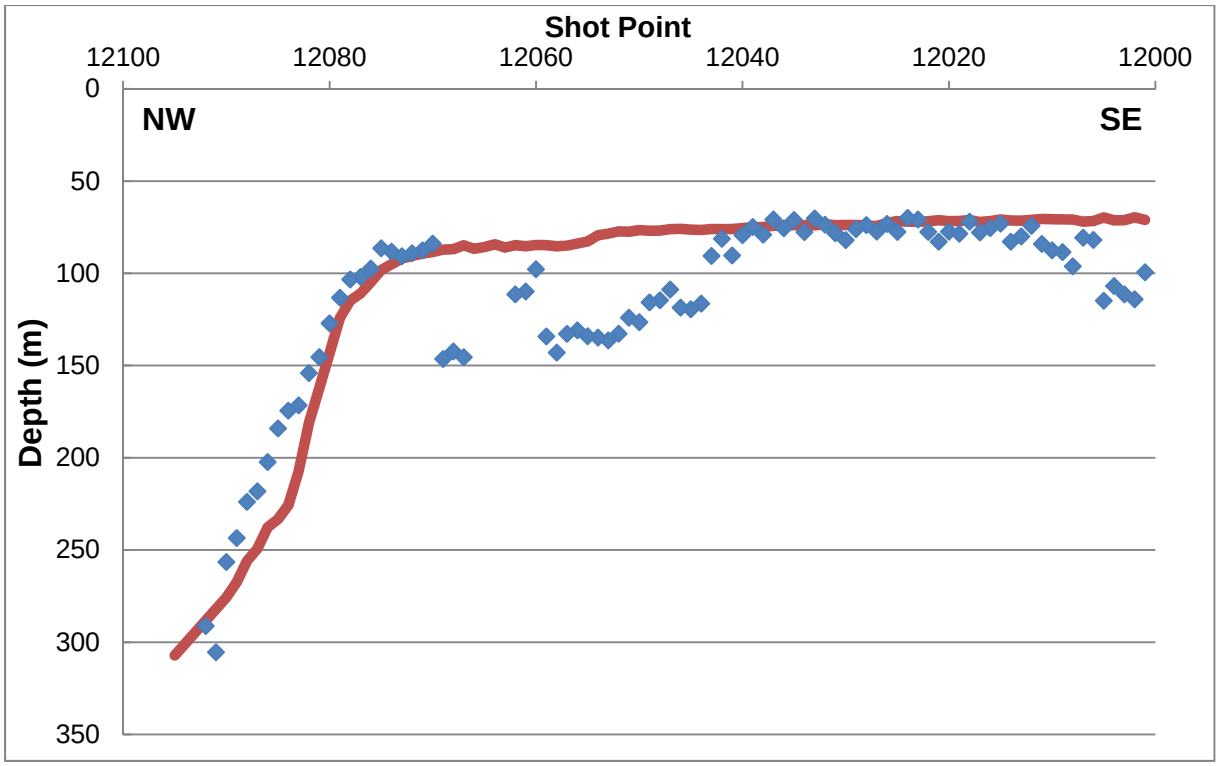

Figure 10v. Results of refraction analysis along Line-12 of Expedition ARA04C showing depth of first refraction in meter below sea-surface (blue diamonds) and seafloor determined from MCS data (dark red line). Shot-numbers increase from SE to NW. The dip and up-slop shooting geometry create too high velocity values, that shift the calculated depth of refractor to depths shallower than the seafloor. No corrections have yet been applied to overcome this problem. The section of deep-refractions correlates to a brightening of sub-seafloor reflections and to a loss of penetration in the 3.5 kHz data (see Figure 12).

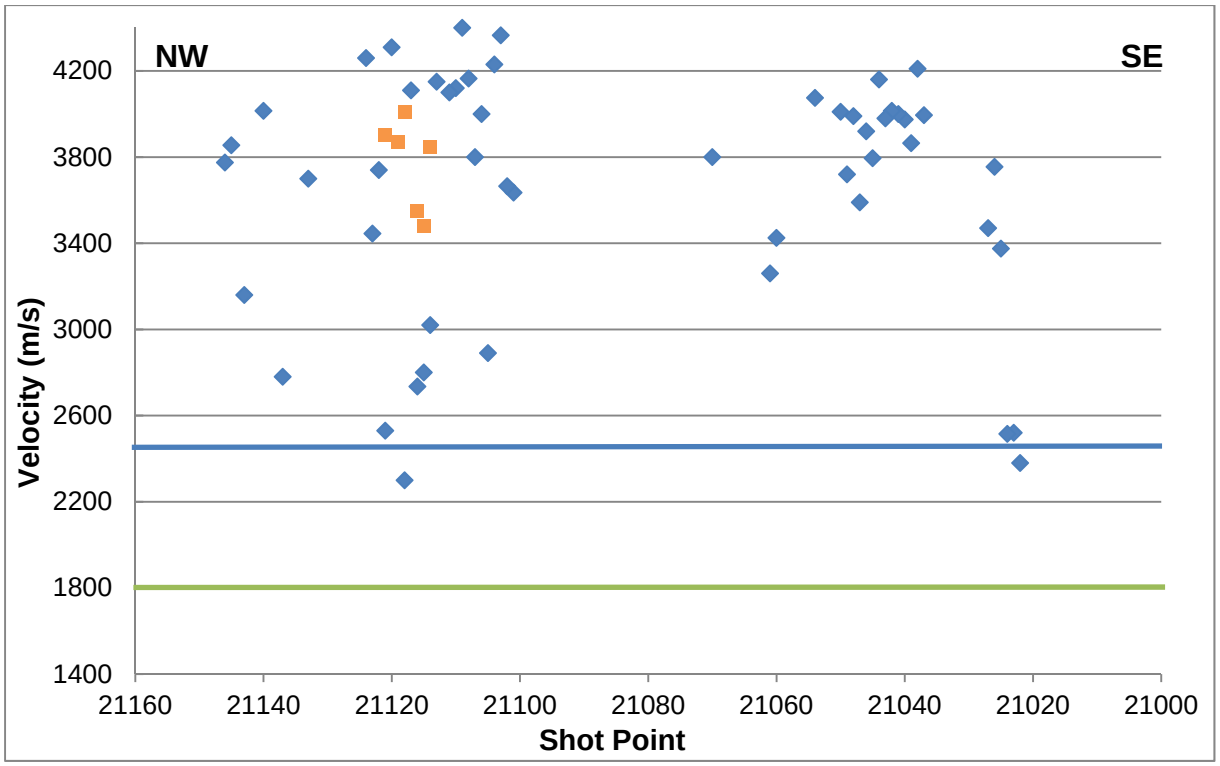

Figure 10w. Results of refraction velocity analysis (hand-picked) from Line-21 of Expedition ARA04C. Velocity only from the first refractor (blue diamonds) are shown together with the 1800 m/s threshold (solid green line) and the threshold of 2500 m/s (blue solid line) used by Pullan et al. (1987) as indicator for ice-bearing sediments and zones of continuous permafrost, respectively. Shot-numbers increase from SE to NW.

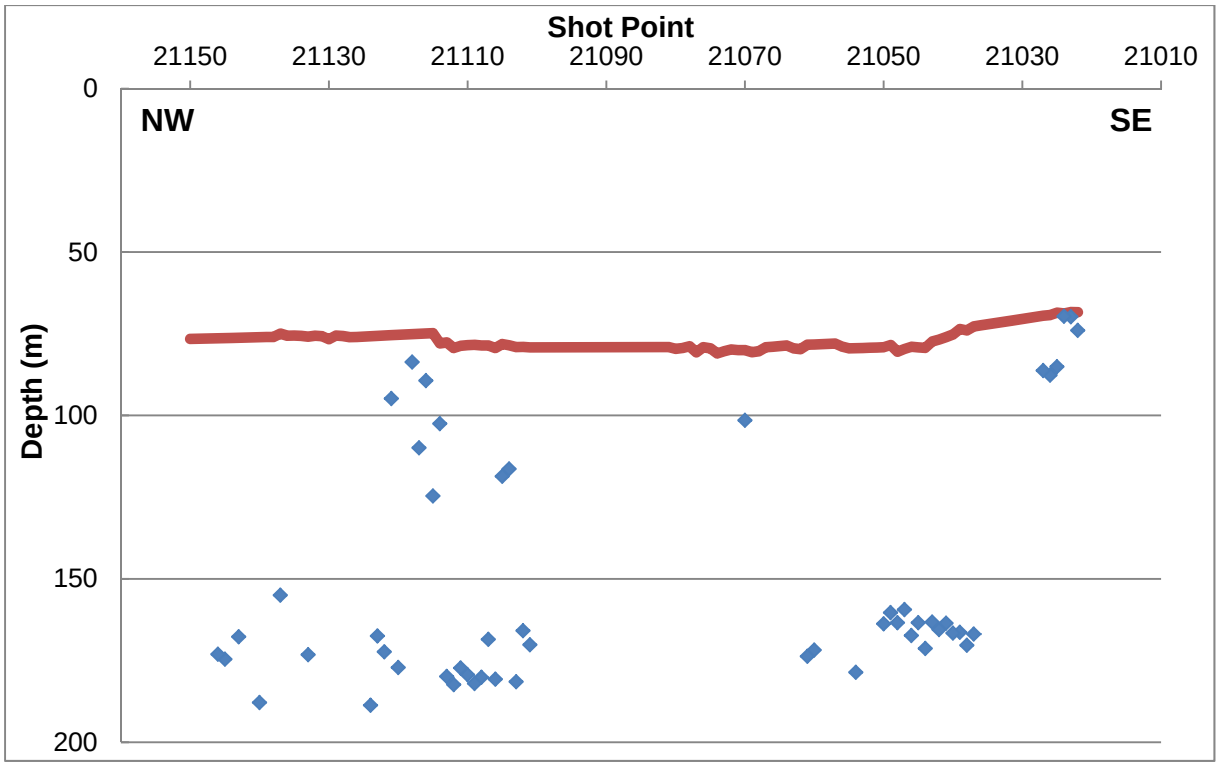

Figure 10x. Results of refraction analysis along Line-21 of Expedition ARA04C showing depth of first refraction in meter below sea-surface (blue diamonds) and seafloor determined from MCS data (dark red line). Shot-numbers increase from SE to NW.

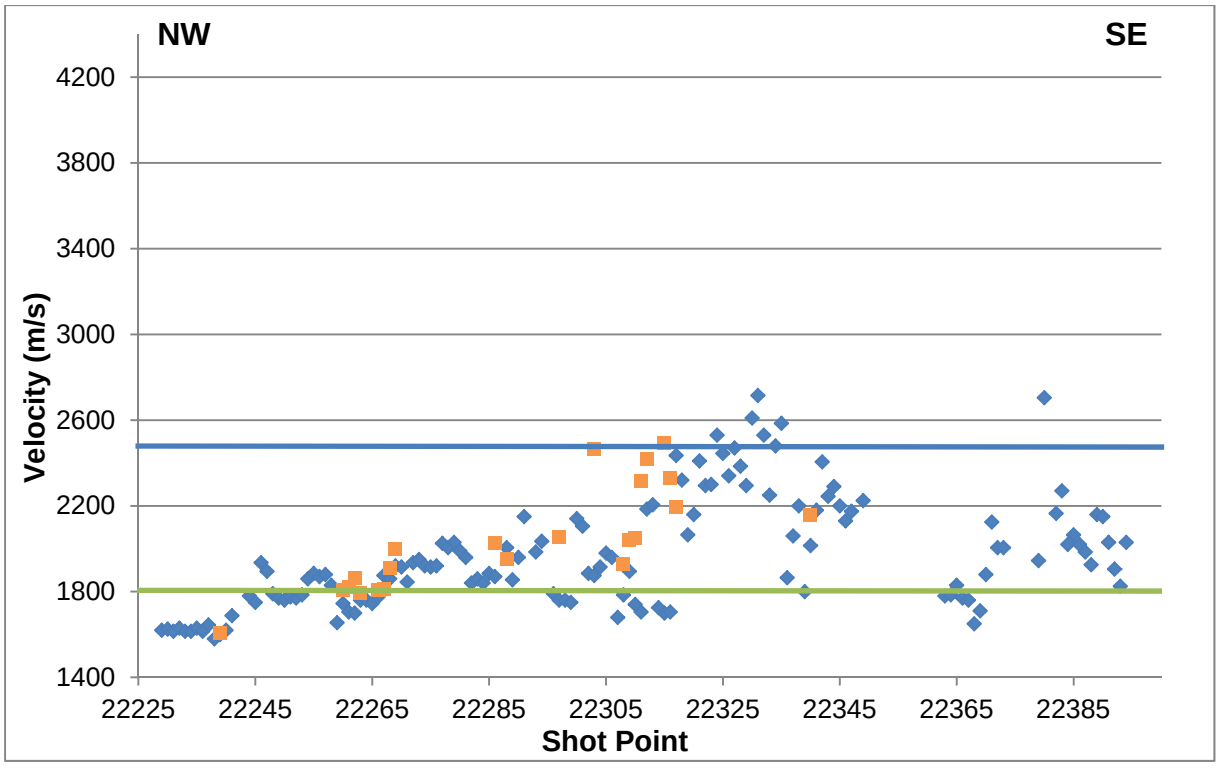

Figure 10y. Results of refraction velocity analysis (hand-picked) from Line-22 of Expedition ARA04C. Velocity only from the first refractor (blue diamonds) are shown together with the 1800 m/s threshold (solid green line) and the threshold of 2500 m/s (blue solid line) used by Pullan et al. (1987) as indicator for ice-bearing sediments and zones of continuous permafrost, respectively. Shot-numbers increase from NW to SE.

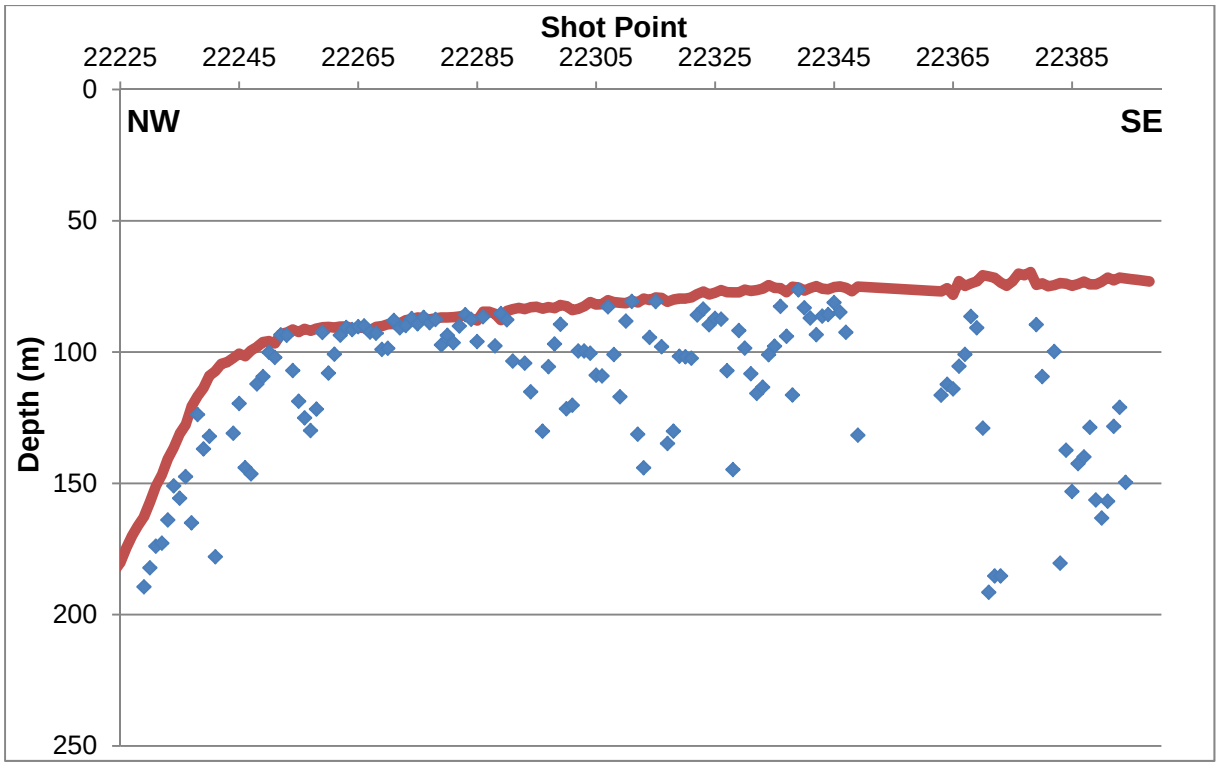

Figure 10z. Results of refraction analysis along Line-22 of Expedition ARA04C showing depth of first refraction in meter below sea-surface (blue diamonds) and seafloor determined from MCS data (dark red line). Shot-numbers increase from NW to SE. The refracted arrivals at the start of the profile are likely from the seafloor. Due to the down-slope shooting geometry (streamer is always over deeper water than the airgun) the velocity obtained is not accurate.

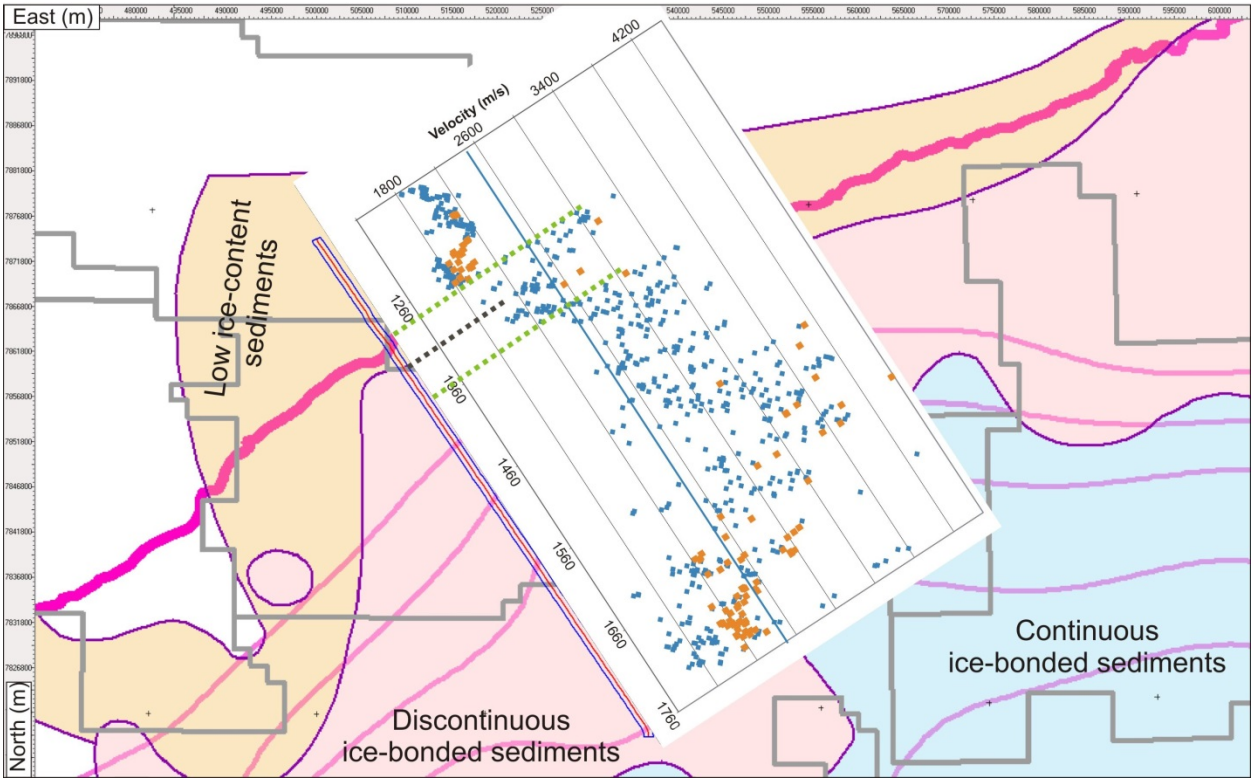

Figure 11a. Map of Pullan et al. (1987) with distribution of ice-bearing sediments and location of Line-1 of Expedition ARA04C. Superimposed are the velocity values (as Figure 10a). The suggested boundary between discontinuous (pink) and low-ice content (yellow) sediments is bracketed by the new velocity results along this line around shot point 1310.

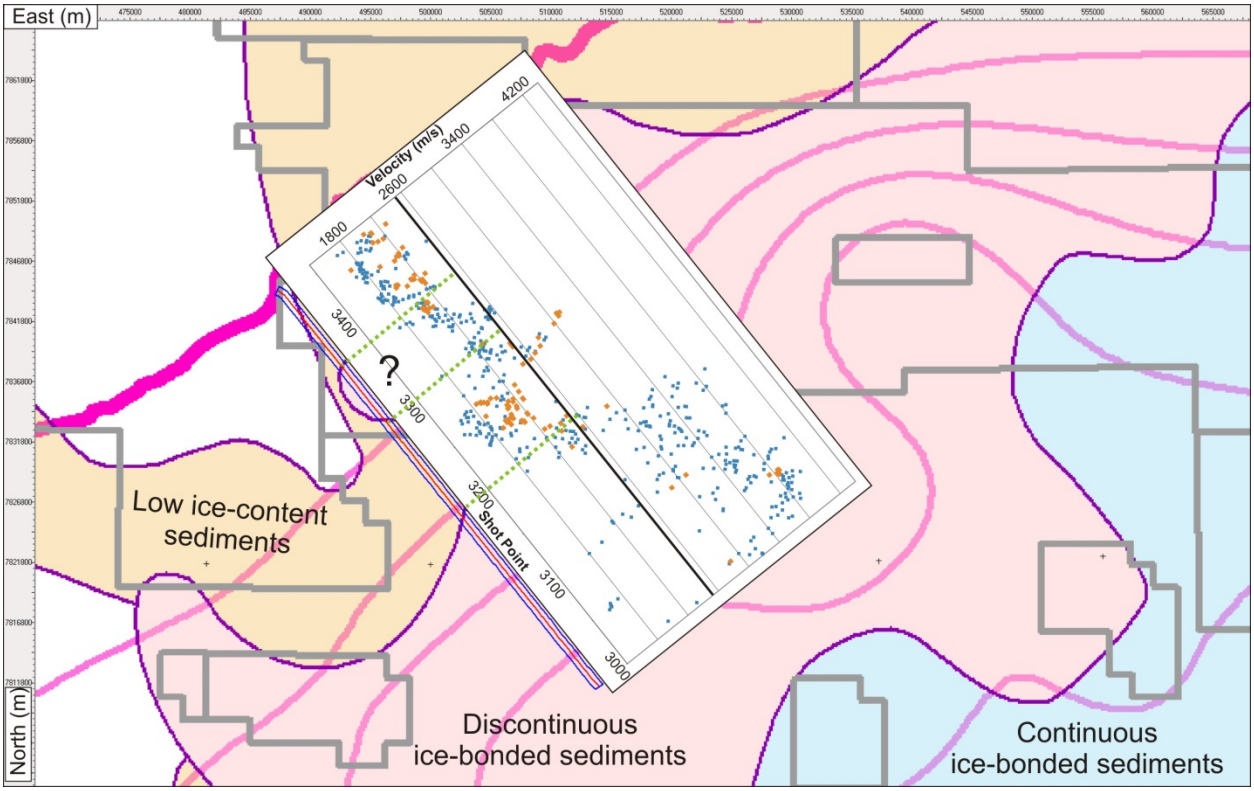

Figure 11b. Map of Pullan et al. (1987) with distribution of ice-bearing sediments and location of Line-3 of Expedition ARA04C. Superimposed are the velocity values (as Figure 10e). The boundary suggested around shot point 3200 between discontinuous ice-bnoded sediments (pink) and low ice-content sediments is confirmed by the new data of Line-3, but the small region between shot points 3300 and 3350 is not as clearly defined as previously suggested.

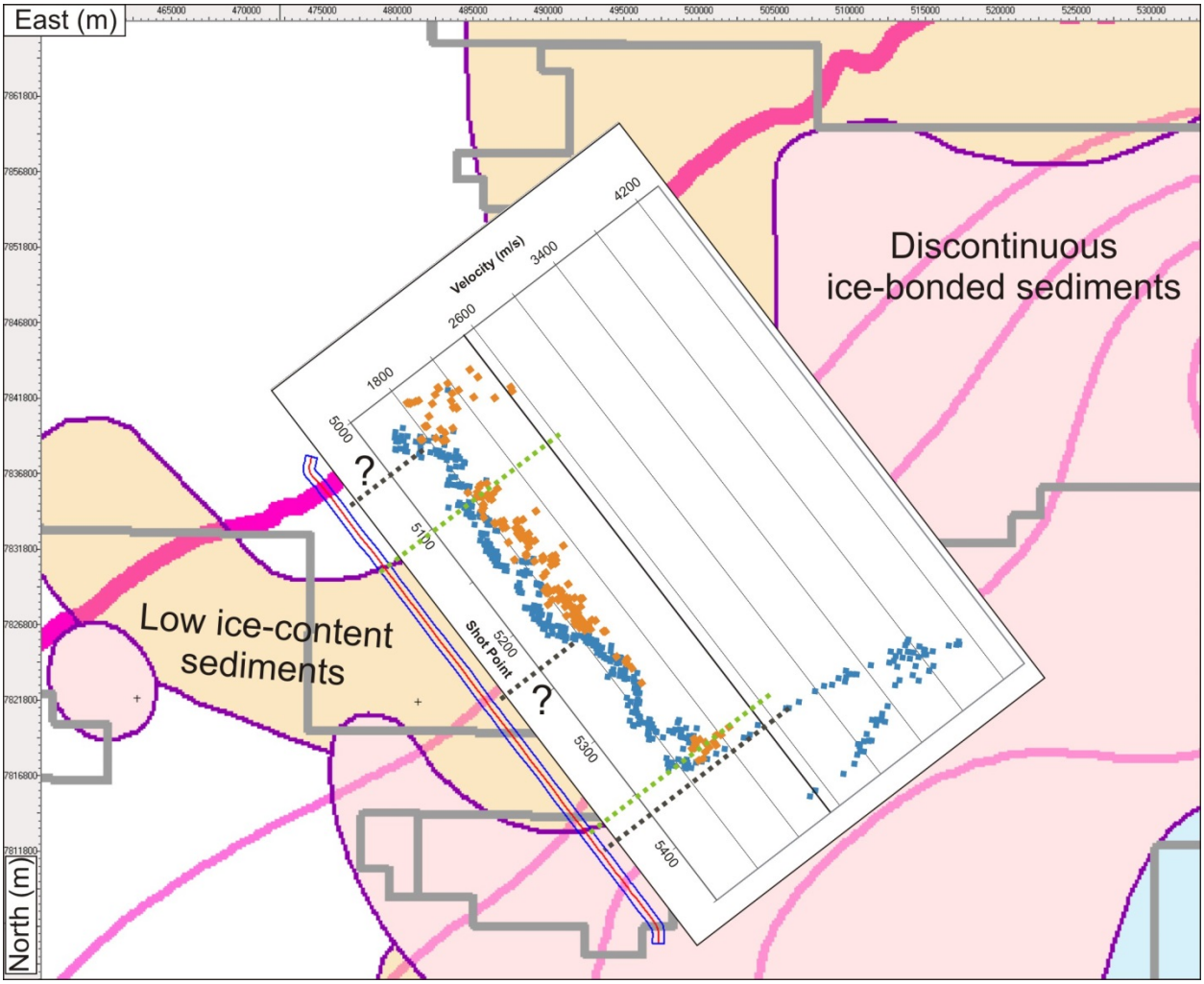

Figure 11c. Map of Pullan et al. (1987) with distribution of ice-bearing sediments and location of Line-5 of Expedition ARA04C. Superimposed are the velocity values (as Figure 10i). The boundary between discontinuous (pink) and low ice-content sediments (yellow) is confirmed by the new velocity data shot point 5350 of this line. However, the extent of the low ice-content sediments is unclear. The new data suggest that the zone extends further into the deeper water in the NW.

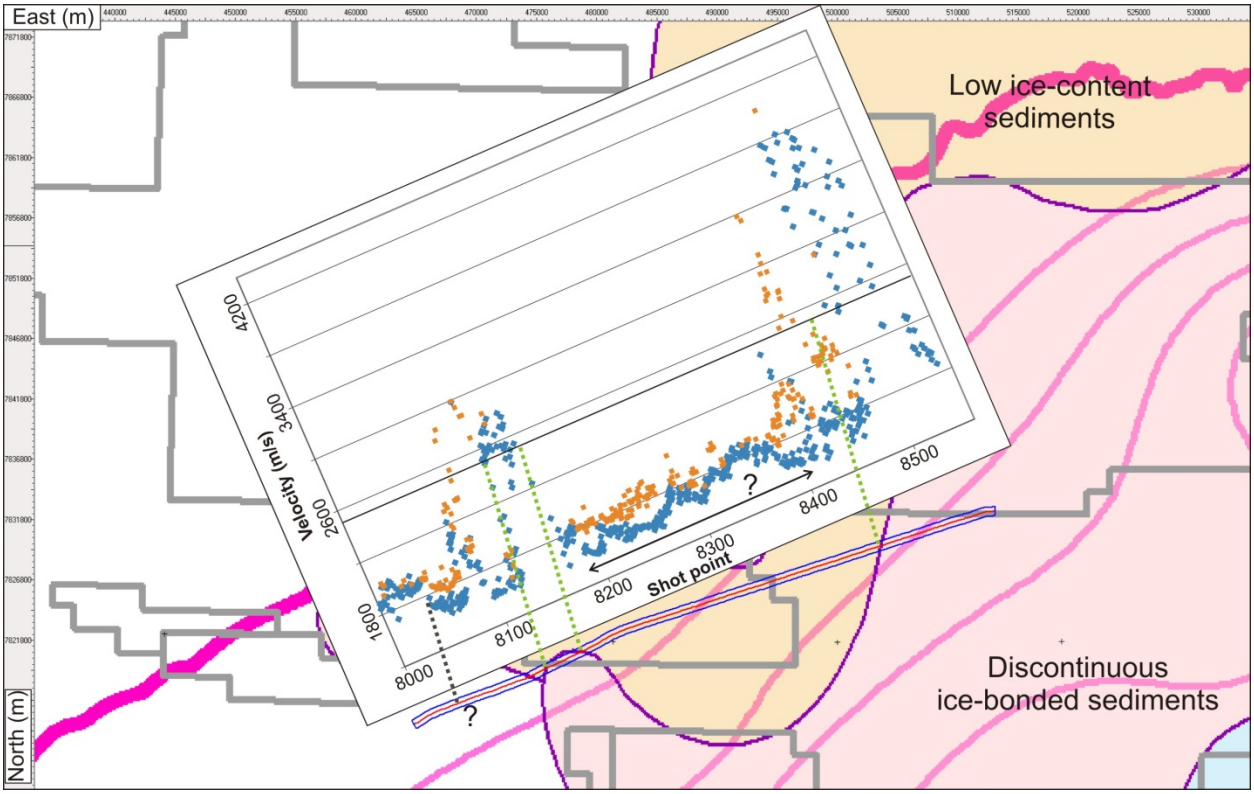

Figure 11d. Map of Pullan et al. (1987) with distribution of ice-bearing sediments and location of Line-8 of Expedition ARA04C. Superimposed are the velocity values (as Figure 10m). The boundaries to the discontinuous ice-bonding sediments (pink zone) previously suggested are confirmed by the new velocity data for all three cases along this line. However, if the first refraction velocity is used only, the extent of low-ice content sediments is not clear. Including velocities from the 2nd refraction along this new line would yield a better match to the previous suggested distribution.

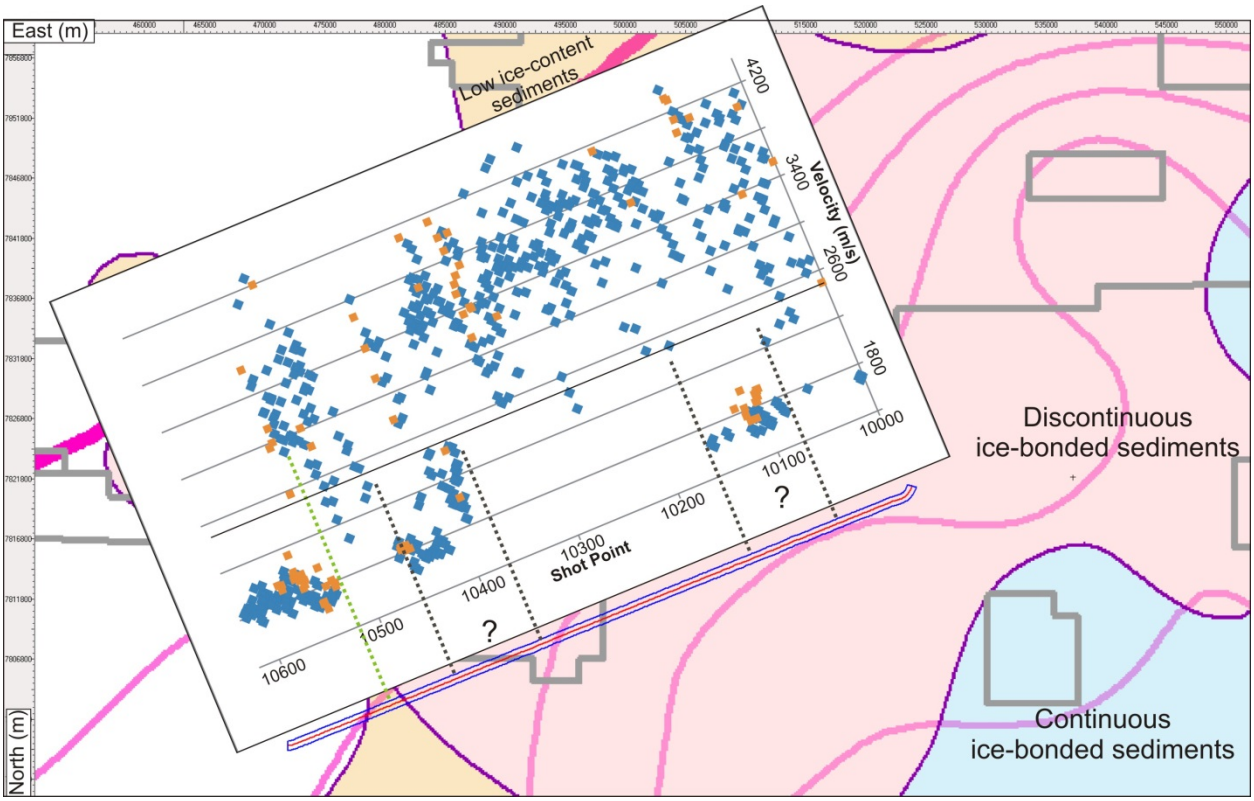

Figure 11e. Map of Pullan et al. (1987) with distribution of ice-bearing sediments and location of Line-10 of Expedition ARA04C. Superimposed are the velocity values (as Figure 10q). The sharp velocity boundary in the SW from velocities around 1800 m/s to values way above the 2500 m/s threshold is confirmed by the new velocity data. However, some minor low-velocity pockets exist along the line, possible related to small-scale channels, previously overlooked.

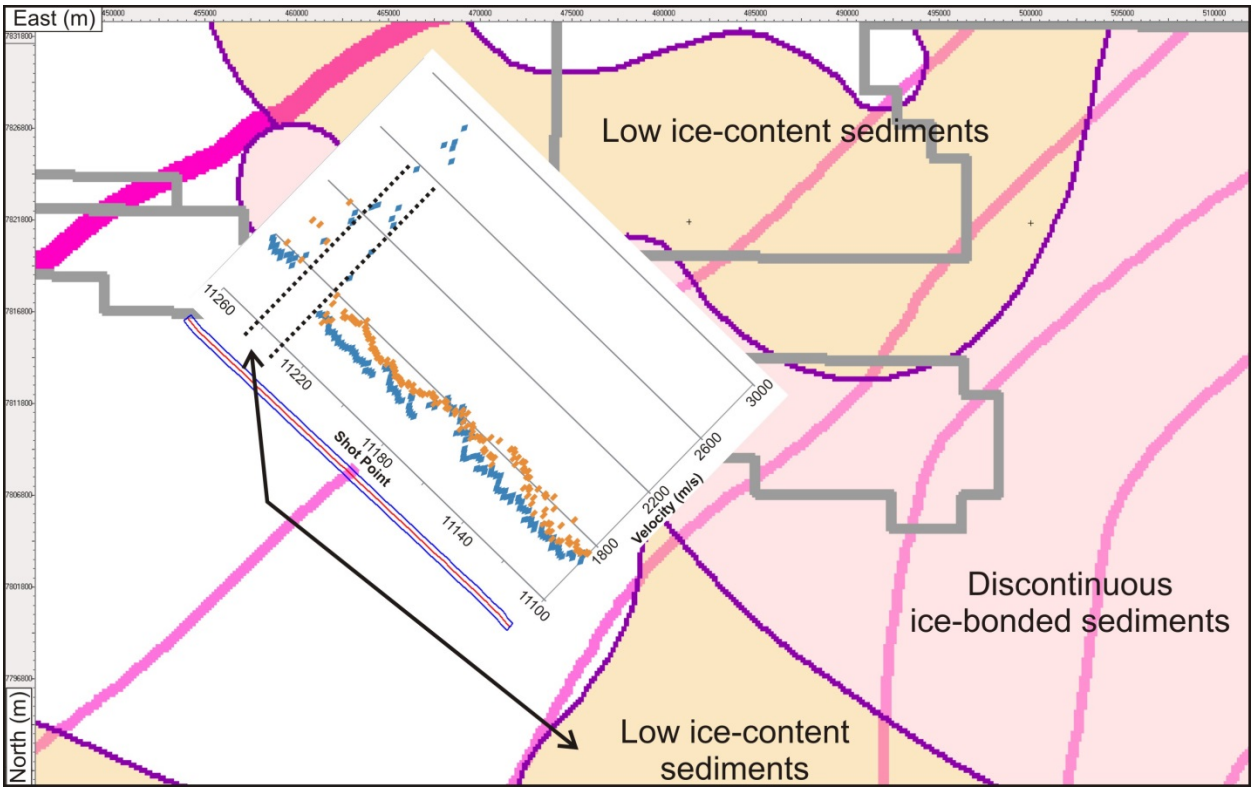

Figure 11f. Map of Pullan et al. (1987) with distribution of ice-bearing sediments and location of Line-11 of Expedition ARA04C. Superimposed are the velocity values (as Figure 10s). The line is outside any zone of potential ice-bearing sediments; however, a short segment as indicated by the black arrow, towards the NW edge of the line may be containing some ice (compare to Figures 12a and 12b).

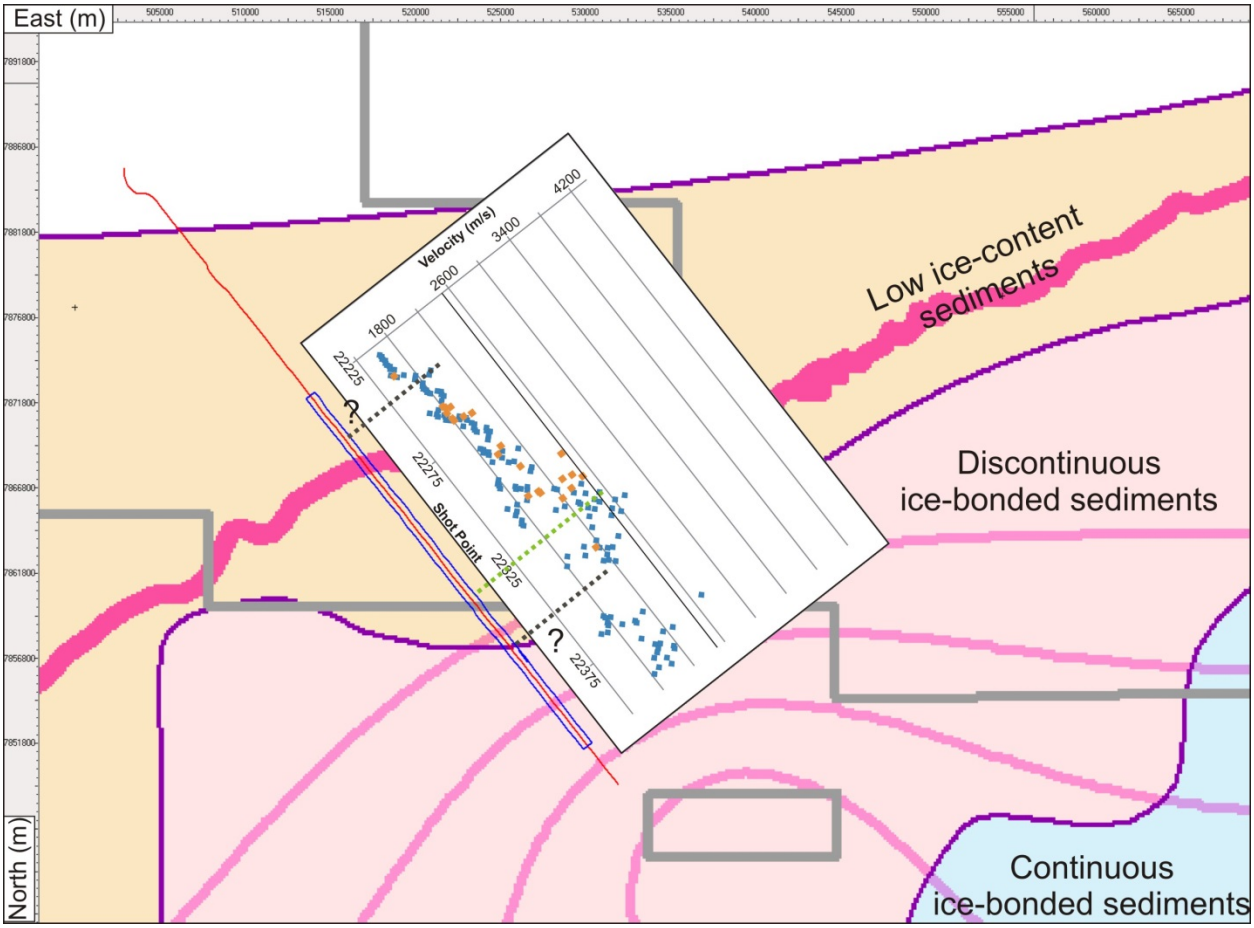

Figure 11g. Map of Pullan et al. (1987) with distribution of ice-bearing sediments and location of Line-22 of Expedition ARA04C. Superimposed are the velocity values (as Figure 10y). The threshold of 2500 m/s (step to discontinuous ice-bonded sediments) is not fully established along this line, but the failing airgun volume may have created conditions that are not comparable to the other lines acquired during the Expedition ARA04C. However, more significantly, the onset of low ice-content sediments (threshold of 1800 m/s) occurs ~15km further inshore than previously suggested along this line (around shot point 22245).

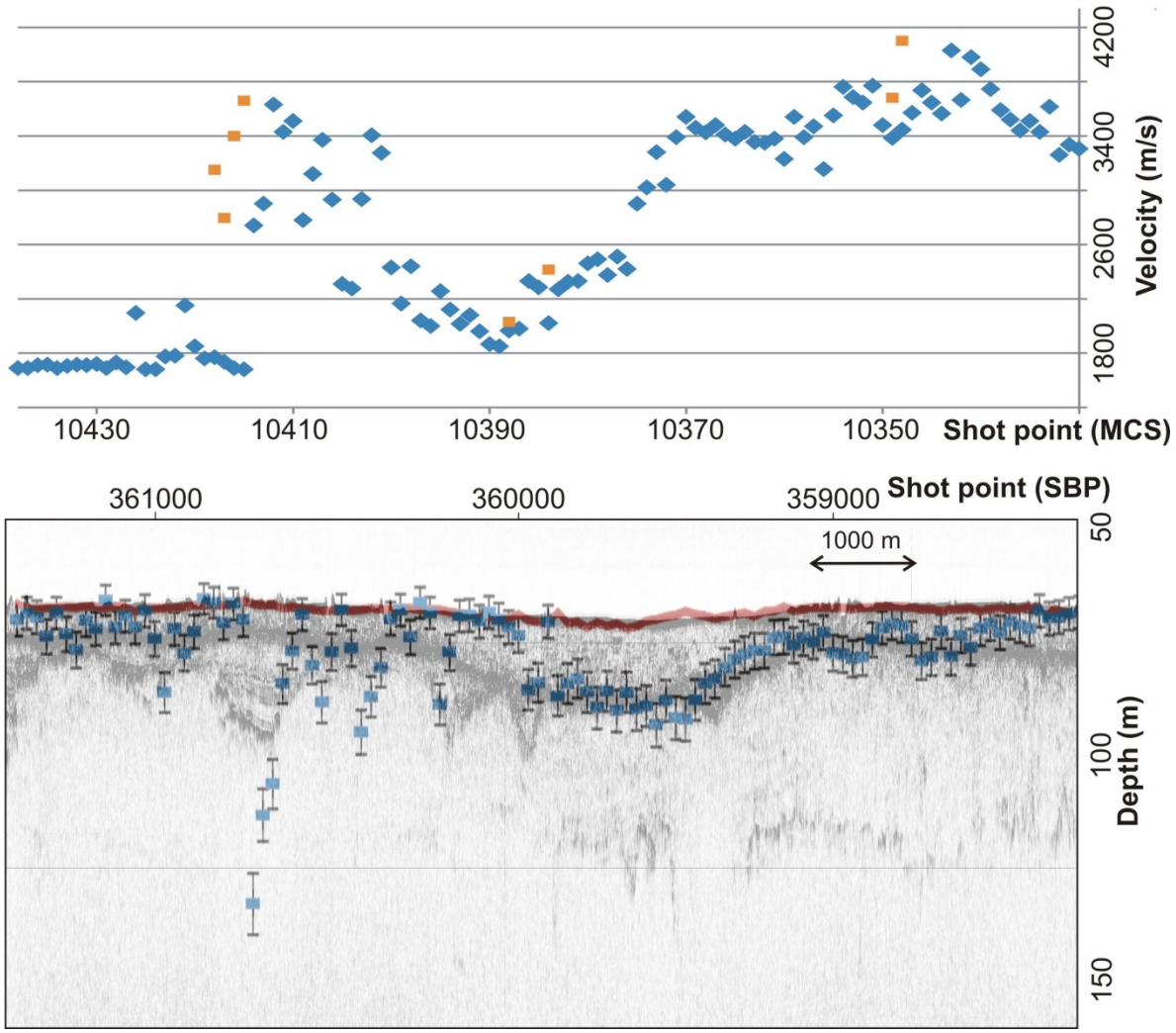

Figure 12a. Comparison of refraction velocity analysis of Line-10 at the occurrence of a sediment-filled channel. Upper panel shows the velocity and lower panel is an overlay of refractor depth (with 5% error bars) on the 3.5 kHz sub-bottom profiler (SBP) data. The depth of the first refractor is ambiguous due to the close occurrence of the unconformity near the seafloor, except for the channel. In this channel, no refraction from the seafloor was identified, which is maybe the result of the 12.5 m trace spacing of the streamer. The refraction may only be seen for one or two channels, before being overwhelmed by the second refraction and thus overlooked. The velocity at the eastern portion of the line are generally above 3000 m/s and represent the unconformity, which may be underlain by some ice-bonded sediments. The ice-content is lost within the channel and re-gained partially further to the east, where a velocity values are more scattered. At the very end of the line, velocity values are much lower and below the 1800 m/s threshold. Here refractions are from the seafloor (therefore explaining the low velocity).

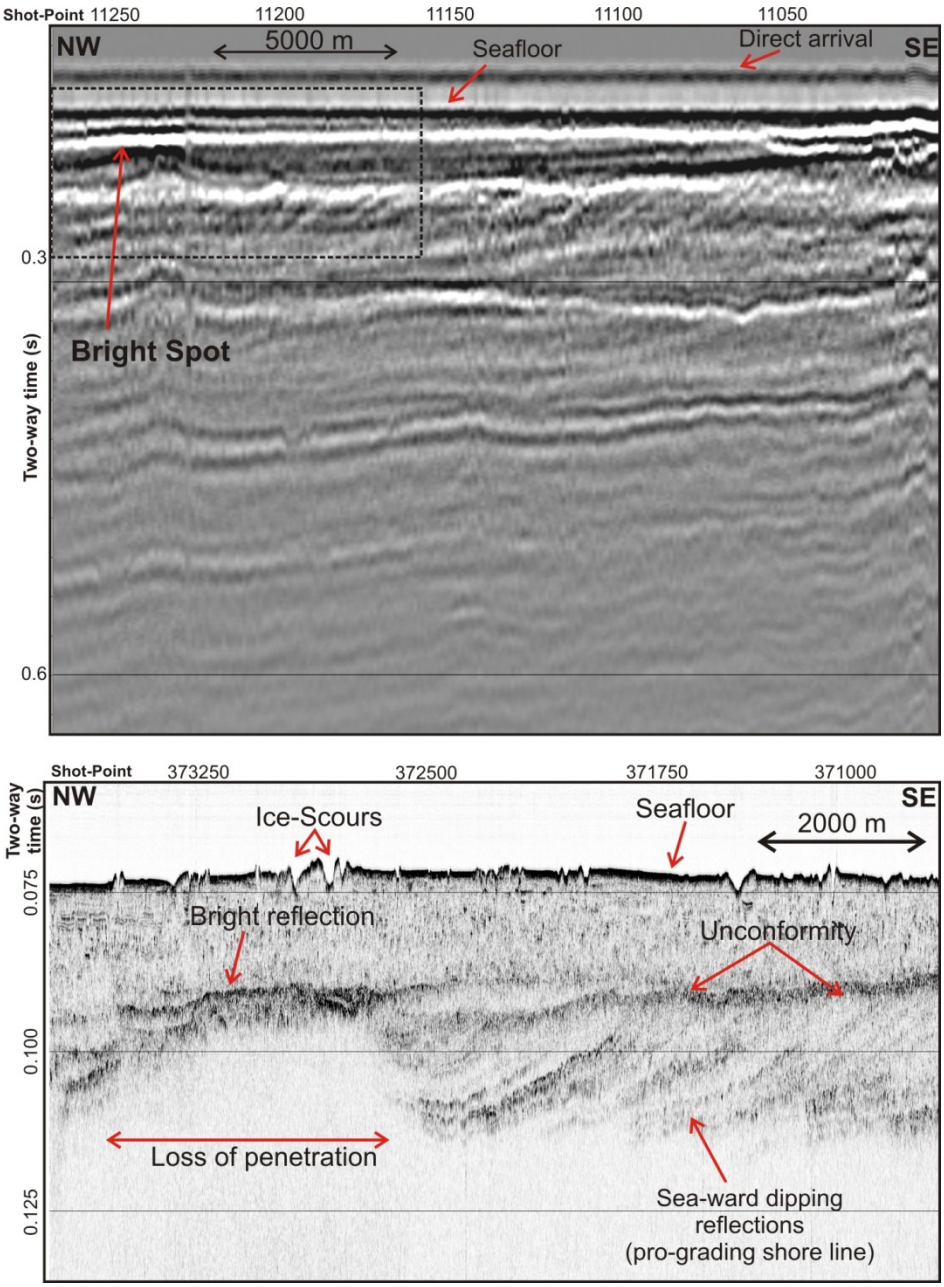

Figure 12b. Comparison of MCS Line-11 (Trace 1 only) and coincident 3.5 kHz data for the occurrence of a bright spot (no polarity reversal). The depth to the top of the bright reflection is roughly converted to 15 (+/- 5) mbsf using the velocity of the top layer from of ~1650 m/s (seafloor velocity prior to the occurrence of the bright spot). This depth correlates within the error-bounds of the refraction analysis to the depth of the refractor seen in Figure 10t at ~10 mbsf.

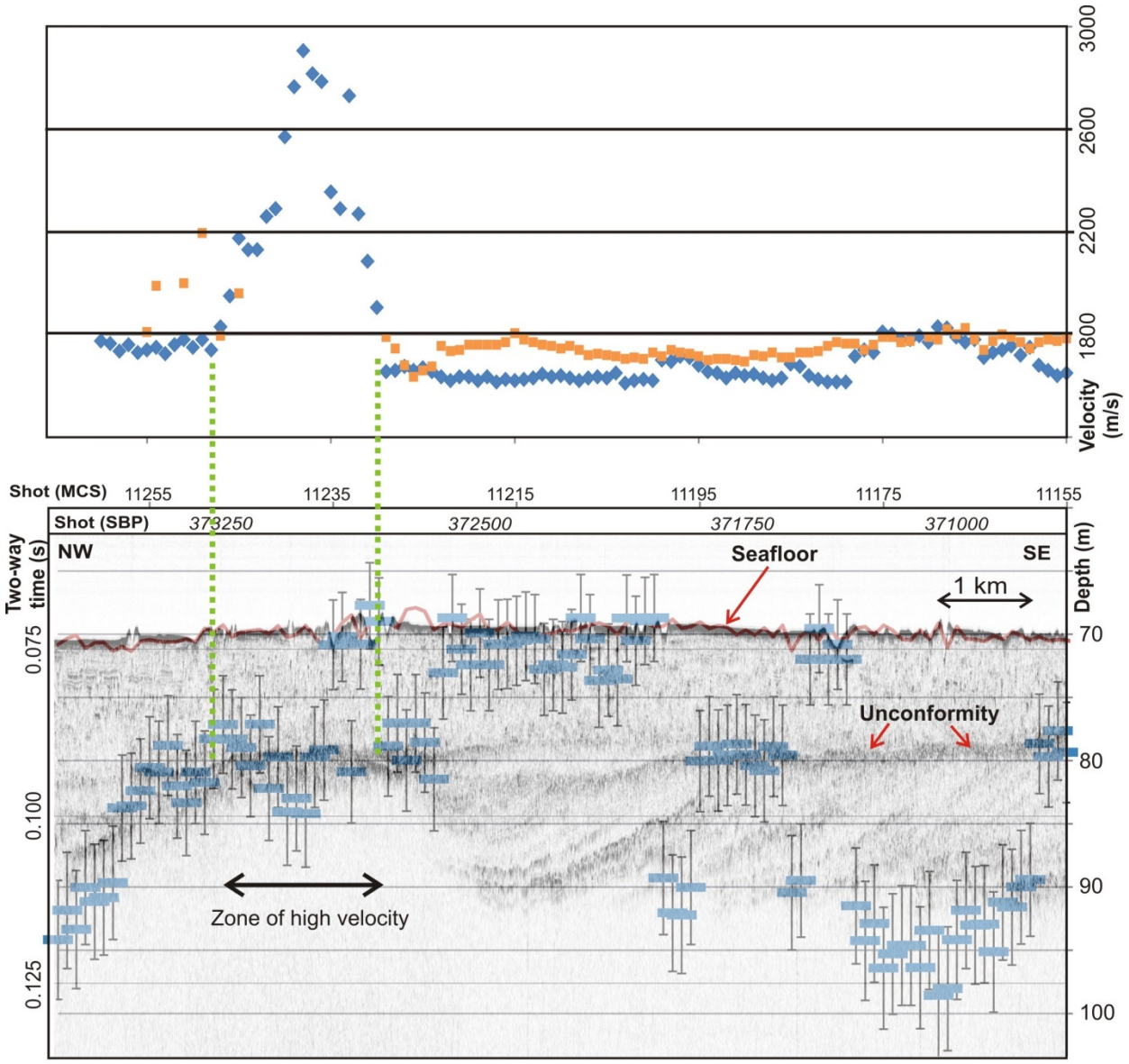

Figure 12c. Comparison of sub-bottom profiler record (as in Figure 12a) and picked refractor depth and velocity from refraction. Refractions either occur from the unconformity (~80 m below sealevel), seafloor (~70 m below sealevel) or from events deeper than the seismic data can image. The high-velocity zone coincides with a bright reflection in the sub-bottom data and loss of penetration underneath. The bright reflection is from the unconformity but the increase in velocity (and reflector strength) suggests some ice-occurrence at or below this unconformity.

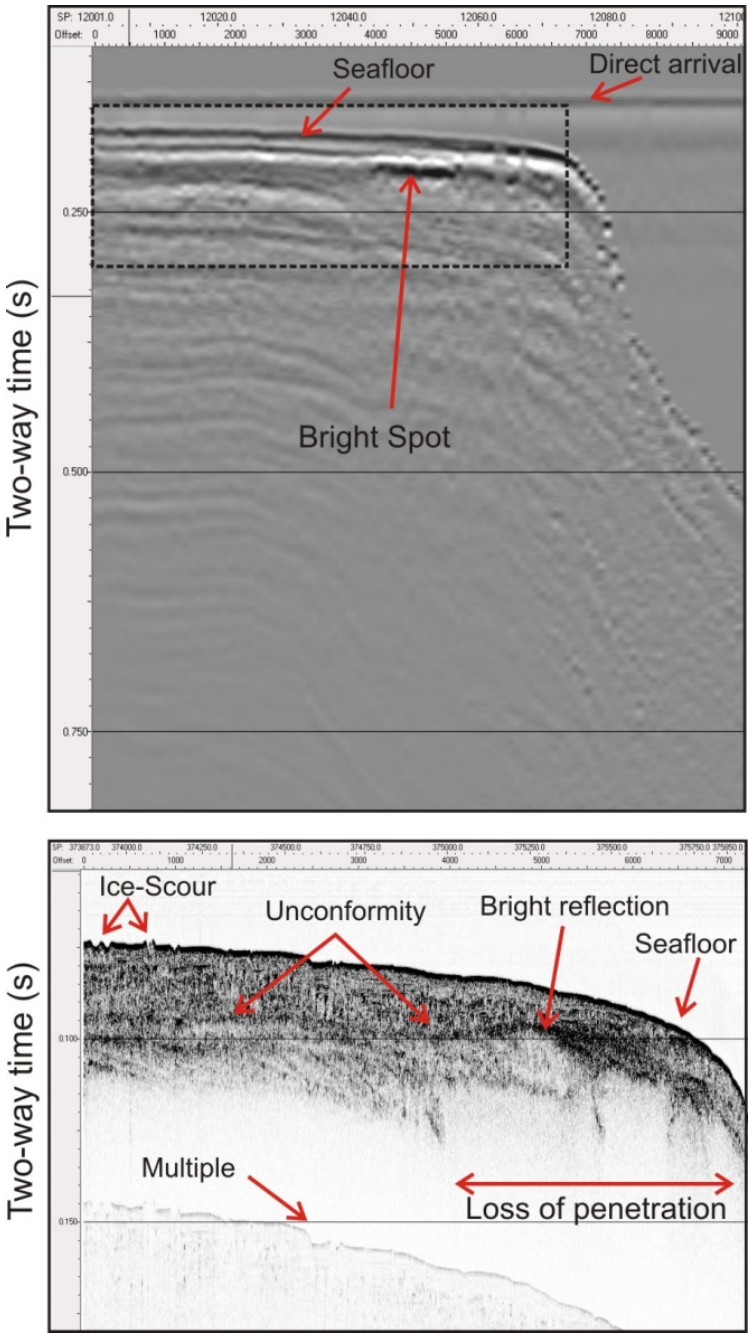

Figure 12d. Comparison of MCS Line-12 (Trace 1 only) and coincident 3.5 kHz data for the occurrence of a bright spot (no polarity reversal). The depth to the top of the bright reflection is roughly converted to 40 (+/- 10) mbsf using the velocity of the top layer from of ~1675 m/s (seafloor velocity prior to the occurrence of the bright spot). This depth correlates within the error-bounds of the refraction analysis to the depth of the refractor seen in Figure 10v (which dips towards the shelf edge from 30 to 45 mbsf).

Shot Interval	93.75 m
Channel Number	120
Group Interval	12.5 m
Source Depth	6 m
Streamer Depth	6 m
Fold of Coverage	8 folds
Work Pressure	150 bar
Recording Length	10.0 sec
Sample Rate	1 ms
File Format	SEG-D

Table 1. Seismic acquisition parameters.